Characterization of ozone deposition to a mixed oak-hornbeam forest. Flux measurements at five levels above and inside the canopy and their interactions with nitric oxide

Angelo Finco[1], Mhairi Coyle[2], Eiko Nemitz[2], Riccardo Marzuoli[1], Maria Chiesa[1], Benjamin Loubet[3], Silvano Fares[4], Eugenio Diaz-Pines[5], Rainer Gasche[6] and Giacomo Gerosa[1,*]

[1] Dipartimento di Matematica e Fisica, Università Cattolica del S. C., Brescia, Italy

[2] Centre for Ecology & Hydrology, Bush Estate, Penicuik, United Kingdom

[3] Institut National de la Recherche Agronomique, Thiverval-Grignon, France

[4] Council for Agricultural Research and Economics, Research Centre for Forestry and Wood, Arezzo, Italy

[5] Institute of Soil Research, University of Natural Resources and Life Sciences (BOKU); Vienna, Austria.

[6] Institute of Meteorology and Climate Research Atmospheric Environmental Research (IMK-IFU), Garmisch-Partenkirchen, Germany

Correspondence to: Giacomo Gerosa (giacomo.gerosa@unicatt.it)

Abstract

A 1-month field campaign of ozone (O_3) flux measurements along a five-levels vertical profile above, inside and below the canopy, was run in a mature broadleaf forest of the Po Valley, Northern Italy. The study aimed at characterizing O_3 flux dynamics and their interactions with nitrogen oxides (NO_x) fluxes from the forest soil and the atmosphere above the canopy. Ozone fluxes measured at the levels above the canopy were in good agreement, thus confirming the validity of the constant flux hypothesis, while below canopy O_3 fluxes were lower than above. However, at the upper canopy edge O_3 fluxes were surprisingly higher than above during the morning hours. This was attributed to a chemical O_3 sink due to a reaction with the nitric oxide (NO) emitted from soil and deposited from the atmosphere, thus converging at the top of the canopy. Moreover, this mechanism was favored by the morning coupling between the forest and the atmosphere, while in the afternoon the fluxes at the upper canopy edge became similar to those of the levels above as a consequence of the in-canopy stratification. Nearly 80% of the O_3 deposited to the forest ecosystem was removed by the canopy by stomatal deposition, dry deposition on physical surfaces and by ambient chemistry reactions (33.3% by the upper canopy layer and 46.3% by the lower canopy layer). Only a minor part of O_3 was removed by the understorey vegetation and the soil surface (2%), while the remaining 18.2% was consumed by chemical reaction with NO emitted from soil. The collected data could be used to improve the O_3 risk assessment for forests and to test the predicting capability of O_3 deposition models. Moreover, this data could help multilayer canopy models to separate the influence of ambient chemistry vs. O_3 dry deposition on the observed fluxes.

1 Introduction

Ozone (O_3) had been widely documented as one of the most dangerous pollutants for plants (Wittig et al., 2009; Matyssek et al., 2012; Gerosa et al., 2015; Marzuoli et al., 2018). The deposition of O_3 on forest ecosystems has been extensively studied over the last 20 years with eddy covariance field campaigns (Padro, 1996; Cieslik, 1998; Lamaud et al., 2002; Mikkelsen et al., 2004; Gerosa et al., 2005, 2009a, 2009b; Launiainen et al., 2013), which were made possible thanks also to the development of fast O_3 analyzers. Measurements carried out in the 1990's were usually short-term field campaigns, while more recent campaigns have extended the observation periods and therefore led to a better understanding of the processes controlling O_3 deposition (Mikkelsen et al., 2004; Gerosa et al., 2005; Fowler et al., 2009; Rannik et al., 2012; Zona et al., 2014; Fares et al., 2010, 2012, 2014; Clifton et al., 2017, Finco et al., 2017).

These studies highlighted that an important deposition pathway is represented by the O_3 uptake by trees through leaf stomata. The O_3 amount entering the stomata strongly depends on the environmental and physiological factors that drive stomata opening (Jarvis, 1976; Emberson et al., 2000), such as, for example, the soil water availability that is positively correlated to the stomatal O_3 flux (Gerosa et al., 2009a; Büker et al., 2012).

Ozone deposition pathways other than plant stomata are usually grouped as non-stomatal deposition, although they include merely physical dry deposition processes and chemical consumption processes due to ambient air chemistry. Among these processes, which still remain to be understood in depth, we find the thermal decomposition on dry surfaces (Cape et al., 2009), the deposition on wet surfaces (Fuentes et al., 1992; Altimir et al., 2004, 2006; Gerosa et al., 2009b), the deposition on soil (Stella et al., 2011), reactions stimulated by light (Coe et al., 1995; Fowler et al., 2001), chemical reactions with NO (Dorsey et al., 2004; Rummel et al., 2007; Pilegaard, 2001; Gerosa et al., 2009b) and chemical reactions with biogenic volatile organic compounds (BVOCs) (Fares et al., 2010; Goldstein et al., 2004).

Also, O_3 deposition dynamics below the forest canopy and their relationship with the above canopy O_3 fluxes are still to be fully understood, since only a few studies have directly measured O_3 fluxes below the canopy. For example, Launiainen et al., (2013) and Fares et al., (2014) used these measurements to assess different deposition pathways and to validate O_3 deposition models, while Dorsey et al., (2004) also included the role of NO_2 fluxes and soil NO emission in the O_3 flux dynamics. Moreover, Goldstein et al. 2004 and Wolfe et al. 2011 highlighted the potential importance of in-canopy reactions of O_3 with BVOCs for O_3 removal from the ecosystem and the formation of secondary organic aerosols (SOA).

There are only a few studies in the literature that have reported O_3 fluxes measured at more than two levels along a vertical profile above and within a forest canopy and, to our knowledge, none of these were made on a mature broadleaf forest.

For example, Dorsey at al. (2004) measured O_3 fluxes at three levels, two above and one below a Douglas fir canopy, and Foken et al. (2012) performed the same measurements at four levels in a Norway spruce forest, one above the canopy, one at the top-canopy and two below the canopy.

On the contrary, vertical gradients of O_3 concentration have been investigated, especially for flux calculation above the canopy with the aerodynamic gradient technique (Kramm et al. 1991; Horvath et al. 1998; Mikklesen et al. 2000; Keronen et al. 2003).

However, a small to high variability of the ozone concentration inside the canopy emerged in many studies (Fontan et al. 1992; Keronen et al. 2003; Utiyama et al. 2003; Gerosa et al. 2005) revealing that uncertainties on the drivers of these gradients inside the canopy still remain. Nevertheless these kinds of measurements are needed for modeling exercises as indicated, e.g., by Walton et al. (1997), Ganzeveld et al. (2002) and Launiainen et al. (2013) who tested the models capability to reproduce the in-canopy profiles of the concentration of O_3 and other gasses.

The major aims of this study were (i) to contribute to the understanding of the diel dynamics of O_3 fluxes and O_3 concentration gradients at five levels above and within a mature broadleaf forest canopy, (ii) to assess the ozone sinks above and within the forest and in particular the amount of O_3 deposited on the different forest layers (upper canopy, lower canopy, understorey, forest floor), and (iii) to evaluate the role of the NO_x exchange on the O_3 deposition, both at the top of the canopy and at soil level.

This work reports data from a joint field campaign, that took place in 2012 in the framework of the European FP7 project ECLAIRE ("Effects of Climate Change on Air Pollution Impacts and Response Strategies for European Ecosystems") in the Po Valley (Italy), one of the most polluted areas in Europe. This campaign also included simultaneous flux measurements of volatile organic compounds (VOCs), particles and ammonia that have been reported in Acton et al. (2016) and Schallhart et al. (2016). To our knowledge, this is the first time that O_3 fluxes have been measured at five levels above and within a broadleaf forest with the eddy covariance technique. The detailed dataset of this campaign will allow future tests on the capability of existing deposition models to correctly predict the O_3 deposition dynamics on forest ecosystems. Moreover, this data could help multilayer canopy models (Ganzeveld et al. 2002 and 2015), to separate the influence of ambient air chemistry vs. O_3 dry deposition on the observed fluxes, and in particular to characterize the in-canopy dynamics involving O_3 reactions with NOx and VOCs.

2 Material and methods

2.1 Site characteristics

Measurements were performed at the Bosco Fontana reserve (45°12'02"N, 10°44'44"E; elevation 25 m a.sl.) located in Marmirolo near Mantua, Italy. The measuring site is a mature mixed oak-hornbeam forest located just in the middle of the Po Valley, one of the most polluted areas of Europe. The forest belongs to a 233 ha natural reserve classified as a Site of Communitarian Importance and Special Protection Zone (IT20B0011) and it is part of the Long-Term Environmental Research (LTER) network.

The upper canopy (dominant tree layer) is composed of the higher trees such as hornbeam (*Carpinus betulus*, 40.45 % of the total surface of the reserve), oak (*Quercus robur*, 17.09 %), red oak (*Quercus rubra*, 9.65 %) and Turkey oak (*Quercus cerris*, 7.06 %) (Dalponte et al., 2007). Some species (*Acer campestre*, *Prunus avium*, *Fraxinus ornus* and *oxycarpa*, *Ulmus minor*, and *Alnus glutinosa* along the small streams) are present but they account for no more than 3% of the total surface.

The lower canopy (dominated tree layer) is represented by the lower trees and it is composed of hazel (*Corylus avellana*), elder (*Sambucus* spp), cornell (*Cornus mas*), hawthorn (*Crataegus oxyacantha* and *monogyna*) and chequers (*Sorbus torminalis*). A thick understorey mostly composed of butcher's broom (*Ruscus aculeatus*, L) is also present.

The average height of the canopy is 26 m and the average single-sided leaf area index (LAI), measured by a canopy structure meter (LAI2000), was 2.28 m^2 m^{-2}, with a maximum value of 4.22 m^2 m^{-2}.

The soil is a Petrocalcic Palexeralf, loamy skeletal, mixed, mesic (Campanaro et al., 2007) according to the USDA classification. The soil depth is 1.5 m with petrocalcic hardened layer between 0.80 and 1 m below the ground; this layer was formed after the gradual deepening of the water table.

The climatic characteristics are typical of the Po Valley, with humid and hot summers (Longo, 2004). The mean annual temperature is 13.2°C (period 1840-1997, Bellumé et al., 1998) and July is the hottest month (24.6°C).

Winds coming from east (E) and north-east (NE) are the most frequent, in particular in spring and summer.

2.2 Measuring infrastructure

A 40 m height scaffolding tower was built inside the natural reserve (45°11'52.27"N, 10°44'32.27"E), at a distance from the edge of the forest ranging between a minimum of 390 m in the south (S) direction and a maximum of 1440 m in the NE direction.

The infrastructure was equipped with instrumentation for four different kinds of measurements: fluxes of energy and matter (O_3, NO_x, CO_2, H_2O) with the eddy covariance technique, soil flux of O_3 and NO_x with dynamic chambers, vertical profiles of gas concentrations (O_3, NO_x) and air temperature and humidity, and additional meteorological and agrometeorological measurements (solar radiation, precipitations, soil temperature, soil heat fluxes and soil water content).

2.3 Eddy covariance measurements of matter and energy fluxes

Four sonic anemometers (see Table 1 for instrument models) were placed on the tower at four different heights: 16 m, 24 m, 32 m and 41 m. A fifth one was installed at 5 m a.g.l. on a pole, 10 m away from the tower, in the west direction. At the top tower level an open path infrared gas analyzer (Model 7500, LI-Cor, USA) was also installed to measure the concentrations of water vapour and carbon dioxide, and at each of the five sampling heights a fast O_3 instrument was installed to measure O_3 vertical fluxes.

Fast O_3 analyzers (Table 1) were based on the reaction between O_3 and a coumarine-47 target which has to be changed after some days because its sensitivity declines exponentially with time (Ermel et al., 2013). Three fast O_3 analyzers, two COFA (Chemiluminescent Ozone Fast Analyzer) and one ROFI (Rapid Ozone Flux Instrument), which broadly followed the design of the GFAS instrument developed by Güsten and Heinrich, (1996), were equipped with a relatively big fan (about 100 L min^{-1}), which resulted in a fast consumption of the coumarin target. The other two instruments, a prototype developed by the National Oceanic and Atmospheric Administration (NOAA, Fast Response Ozone Monitor, Bauer et al., (2000)) and the commercial Fast Ozone Sensor (FOS, Sextant, NZ), both made use of a small membrane pump (2.5 L min^{-1}) and thus had a

lower consumption of the coumarin targets compared to the other instruments. For this reason, the coumarin targets were changed every 5 days for the COFA and the ROFI and every 10 days for the FROM and the FOS. In both cases the coumarin targets were pre-conditioned just before use by exposing them to a concentration of 100 ppb of O_3 for two hours.

Above-canopy fluxes of NO were measured at 32 m by means of a CLD780TR fast analyzer (Ecophysics, CH) based on the chemiluminescence reaction between O_3 and NO. The air to be analyzed was drawn from 32 m through a 3/8 ID Teflon tube main line at 60 L min^{-1} to the analyzer placed at the bottom of the tower. The analyzer was sub-sampling at 3 L min^{-1} from the main sampling line. The CLD780TR was calibrated with an 80 ppb standard produced using a dilution system (LNI 6000x, S) and a standard NO cylinder (18 ppm), at the beginning of the experiment, and then weekly.

All the fast instruments and the sonic anemometers were sampled at 20 Hz through a customized LabVIEW (National Instruments, IRL) program and data were collected and stored in half-hourly files.

2.4 Soil NO, NO_2 and O_3 flux measurements

Fluxes and concentrations of NO, NO_2 and O_3 at the soil-atmosphere interface were determined by use of a fully automated measuring system as described in detail elsewhere (Butterbach-Bahl et al., 1997; Gasche and Papen, 1999; Rosenkranz et al., 2006; Wu et al., 2010). Briefly: five dynamic measurement chambers and one dynamic reference chamber were installed at the site. Dimensions of the chambers were: 0.5 m x 0.5 m x 0.15 m (length x width x height). In contrast to the measuring chambers, the reference chamber was sealed gastight against the soil surface using a plate made of Perspex. A 1-hour resolution was chosen for flux measurements. Every chamber was closed and measured for 6 minutes, and before each sampling of a measuring chamber the reference chamber was sampled, resulting in a measuring cycle of 60 minutes. During sampling, the air from the chambers was sucked at a constant rate of 50 L min^{-1} and transported via PTFE tubing (inner diameter: 10 mm, length 20 m) to the analyzers. NO and NO_2 concentrations were determined using a chemiluminescence detector CLD 770 AL equipped with a photolytic converter (Models CLD 770AL and PLC 760, Ecophysics, CH), and O_3 concentrations were determined using an UV O_3 analyzer (model TE49C, Thermo Environmental Instruments, USA). Corrections for initial concentrations of NO, NO_2 and O_3 at the outlet of each chamber and calculation of fluxes of NO and NO_2 was performed according to Butterbach-Bahl et al. (1997). Calibration of the chemiluminescence detector was performed weekly using 40 ppb NO in synthetic air produced by dilution of standard gas (4 ppm NO in N_2) with synthetic air (80% N_2, 20% O_2) using a multi gas calibrator (model 6100, Environics, USA). Efficiency of photolytic conversion of NO_2 to NO was determined at least weekly as described in detail by Butterbach-Bahl et al. (1997).

2.5 Vertical profile of O_3 and NO_x concentrations and air temperature and humidity

A computer driven system of Teflon tubes and solenoidal Teflon valves was used to characterize the vertical concentration profile of O_3 and NO_x above and within the canopy at 6 heights: 5 m, 8 m, 16 m, 24 m, 32 m and 41 m. The air samples drawn through 3/8 ID Teflon tubes (all of them 50 m long) from each level by a 30 L min^{-1} pump were sequentially sent to an UV O_3 photometer (model 49C, Thermo Scientific, USA) and to a NO_x chemiluminescence analyzer (model 42C, Thermo

Environmental Instruments, USA) lodged in an air-conditioned container at the bottom of the tower. Both analyzers were sub-sampling at 2 L min^{-1} out of the 3/8 ID sampling lines.

All the tubes were insulated and continuously purged. Each level was sampled for 4 minutes after 1-minute wait to let the analyzers stabilize and then concentration data were recorded as half-hourly averages with a customized LabVIEW program (National Instruments, USA).

The O_3 gradient analyzer was calibrated against a reference photometer before and after the field campaign and no significant deviation from the first calibration was observed. The NO_x analyzer was calibrated with the same procedure described above for the Ecophysics CLD780TR at the beginning of the experiment and then weekly.

Additional O_3 and NO_x concentrations at 0.15 m were also available from the soil chambers system previously described.

The O_3 concentrations at 5 m, 16 m, 24 m, 32 m and 41 m were also used as absolute O_3 reference for the fast O_3 instruments all of which change sensitivity sufficiently fast to require constant calibration against a slow response absolute instrument.

Five temperature and relative humidity probes (model HMP45, Vaisala, Finland) were installed, at the higher tower levels (16 m, 24 m, 32 m and 41 m) and, additionally, at 11 m. All these probes were connected to a data logger (CR23x, Campbell Scientific, USA), sampled once per minute and stored as half-hourly averages. Two additional temperature sensors (PT100, Campbell Scientific, USA), were available at 1.5 m and 0.15 m a.g.l. and data were collected with the same personal computer used for the control of the dynamic chamber system.

2.6 Additional meteorological and agrometeorological measurements

On the top of the tower a net radiometer NR-lite (Kipp & Zonen, NL), a BF5 sunshine sensor for total and diffuse PAR (Delta-T Devices, UK), a PTB101B barometer (Vaisala, Finland) and a rain gauge (model 52202, Campbell Scientific, USA) were mounted.

Several soil probes were installed at a distance of 20 m from the bottom of the tower: four reflectometers for soil water content (model TDR 616, Campbell Scientific, USA), four soil heat flux plates (model HFP01SC, Hukseflux, NL) and four soil temperature probes (PT100, GMR Strumenti, I). All these sensors were connected to a data logger (CR13x, Campbell Scientific, USA), sampled with a 1-minute resolution and data were stored as half-hourly averages.

2.7 Measuring period

The measuring campaign began on 12th June and ended one month later, on 11th July 2012. From the 12th June to the 23rd June three fast O_3 instruments (ROFI, FROM and one of the two COFA samplers) were all placed above the canopy at a height of 32 m in order to compare them and to characterize their performances ("Intercomparison period"). The COFA installed at the top of the tower started its measurements on 12th June and was not moved to the 32 m level for the intercomparison because it was already compared with the second COFA before the campaign.

The intercomparison test allowed to verify the agreement between the three instruments, and the average relative standard deviation was below 10%. Considering the intrinsic variation due to the different behavior of individual coumarin targets no

systematic correction was applied. The sextant analyzer, the one employed at 5 m, was calibrated after the field campaign against one of the two COFA. Also in this case, no significant deviation was observed and no corrections were applied.

On 24th June each fast O_3 instrument was moved to a different level (Table S1) to begin the flux profile measurements, which ended on the 11th July ("Flux Profile period"). Every average diel course showed in the results section is referred to this period.

The FOS installed at 5 m was checked after the field campaign by running it in parallel with the COFA previously used at 32 m in the intercomparison period.

2.8 Data processing

The flux measurement technique adopted here was the eddy covariance method (Foken, 2008), which states that fluxes are equal to the covariance between the vertical wind component and the scalar of interest (Arya, 2001). An averaging period of 30 minutes was chosen for the calculation of the covariances.

Despiking. The data series were divided into 2 minutes sub-series and for each of them block average and standard deviation were calculated. Spikes were identified as the instantaneous data that exceeded the average of each sub-series for more than 3.5 times the standard deviation, as proposed by Vickers and Mahrt (1997). Spikes were removed from the series and the data were then gap-filled by a linear interpolation.

Rotations. Two axis rotations were applied to the instantaneous wind components to align u with the mean flow over the averaging period: the first rotation aligned the horizontal wind to the 30 minutes average u component (this rotation forces $\bar{v} = 0$), and the second one to rotate the xy plane in order to zero the 30 minutes average vertical component of the wind ($\overline{w} = 0$) (McMillen, 1988; Wilczak et al., 2001). These rotations corrected the little imperfections in the vertical alignment of the sonic anemometers and prepare data for flux calculations. Samples with a second rotation (vertical tilt) angle greater than 15° were discarded.

Linear detrending. The fluctuations of each parameter (w', T', O_3') were calculated as the differences of each instantaneous value from the best linear fit (minimum square) of the considered time series during each half hour (Lee at al., 2004).

Time-lag determination. O_3 fluxes were calculated using a fixed time-lag between the vertical wind time series and the O_3 concentration one. For each fast instrument the time lag that maximized the cross-covariance function between the vertical component of the wind and the O_3 concentrations was identified and the more frequent lag was used in the calculations for each half-hourly average flux.

Elimination of the kinematic fluxes below the error threshold. The error threshold was quantified for each half-hourly data series by following the methodology proposed by Langford et al., (2015). The standard deviation of the auto-correlation function was calculated for each half-hourly data chunk, with lags ranging between 30 and 60 seconds from the characteristic time lag of each instrument. Kinematic fluxes lower than three times the standard deviation (relating to the 95th percentile) were discarded.

Frequency loss correction.

The frequency loss correction factors for the different fast O_3 analyzers were calculated using the experimental transfer function approach following the methodology proposed by Aubinet et al. (2000). This method considers the normalized cospectra for sensible heat as unaffected by frequency loss or, at most, affected by frequency loss that are negligible with respect to those related to the other considered scalar (O_3, NO, H_2O). The transfer function is calculated for each half-hourly average as the ratio between the normalized cospectra of O_3 (in our case) and the normalized cospectra of sensible heat, then fitted with a Gaussian type function (Aubinet et al., 2001), and thus used to calculate a correction factor for each instrument. For further details, please refer to Aubinet et al. (2012).

Schotanus and WPL corrections. Fluxes of sensible heat (H), latent heat (LE) and trace gases were corrected for air density fluctuations. The formulation adopted for the correction of H was the one proposed by Schotanus et al., (1983) while the formulation used for LE and trace gases was the one proposed by Webb et al., (1980).

Calculation of fluxes in physical units. Fast O_3 concentration data –acquired as voltages- and fast NO concentration data –acquired as counts per second- required additional processing to calculate quantitative fluxes in physical units. First, for all the fast O_3 instruments the target zero V_0 (Muller et al., 2010) – i.e. the output voltage when O_3 concentration is 0 ppb – was identified for each coumarin target employed. Then the O_3 fluxes were calculated by the following equation (Muller et al., 2010):

$$F_{O3} = \frac{\overline{w'V'}}{\bar{V} - V_0} C_{O3} \quad (1)$$

where $\overline{w'V'}$ is the covariance between the vertical wind component and the raw output voltage of the fast O_3 instrument, $\bar{V}$ is the half-hourly average output voltage of the instrument, V_0 is the zero target, identified for the considered half hour, and it represents an estimation of the voltage at zero O_3 concentration, and C_{O3} is the O_3 concentration measured by the reference O_3 analyzer averaged over the same period. The data of the two hours following each target change were excluded in order to allow the target sensitivity to stabilize after the target installation.

Similarly, NO fluxes (F_{NO}) were calculated using the following equation:

$$F_{NO} = \frac{\overline{w'cps'}}{S_{NO}} \quad (2)$$

where *cps* (counts per second) is the raw signal of the NO analyser photomultiplier and the prime stands for variation around the mean, and S_{NO} is the sensitivity of the analyzer determined by calibration against standard gases. S_{NO} ranged from 10000 to 12000 cps/(µmol m^{-3}).

Ozone storage. O_3 fluxes measured by eddy covariance were corrected for the O_3 storage every half hour. The O_3 storage is the temporal variation of the vertical O_3 profile below the measuring point located at the height z_m. It does not represent a true O_3 removal or production process, but only a temporary accumulation of O_3 in the air column below the measuring point or a temporary O_3 release out of the same air column. For a non-reactive tracer, the proof of it is that the storage integrated over a whole day is null. The calculation of the O_3 storage is necessary for a proper determination of the O_3 deposition processes.

The correction of the O_3 fluxes for the storage was made by means of the following equation (Rummel et al., 2007):

$$F_{StorO_3} = F_{O_3} + \frac{\partial}{\partial t} \int_0^{z_m} O_3(z)dz \quad (3)$$

where F_{StorO_3} are the O_3 fluxes corrected by storage, F_{O_3} are the measured O_3 fluxes obtained with the Eq. (1), and the second term on the right represents the O_3 storage term. For a reactive tracer like O_3 some of the stored gas may be destroyed by reaction with NO and potentially with VOCs before being re-released to the air space above, and thus, Eq. (3) must be considered an approximation. A fully resolving 1D chemistry and exchange model would be required to quantify the effect of chemistry on the storage term more fully.

Stationarity check. Finally, the stationarity of each half-hourly sample was verified following the methodology of Foken and Wichura (1996) and the non-stationary data were discarded.

3 Results

3.1 Microclimate

Significant rainfalls had cooled the air before the beginning of the field campaign so that, air temperature increased significantly only during the first days and then remained stable (Figure S1a). The average temperature at the top of the tower was 25.9 °C, while the lowest average temperature (23.1 °C) was recorded at 0.15 m. The maximum temperature during the whole period was 36.2 °C which was observed at the top of the canopy (24 m).

On average the minimum temperature was registered during the night, at around 3:00 (local solar time, always the same hereafter) (Figure S1b) for the 11 and 24 m levels and one hour later for all the other levels, with values ranging from 19 °C to 21 °C. Two significant rainfall events occurred in the final part of the campaign accounting for a total of 108 mm of rain, but these did not significantly affect the air temperature (Figure S1a). In general, most of the days were sunny (only three days were partially cloudy) and humid, with nighttime peaks of relative humidity up to 80% and diurnal minima around 40%. Specific humidity q ranged, on average, between 10 and 13 g_{H_2O}/kg_{air} (Figure 1a). Below canopy levels (≤ 16 m) showed higher q than the above canopy levels early in the morning, at around 6:00, and from 13:00 to 21:00, while the top-crown level (24 m) showed the lowest q values from 4:00 to 16:00. Similar specific humidity values were registered for the above canopy levels, with slightly higher values at 41 m.

The wind blew mostly from the E or the W directions, with about 50% of the data in these directions (Figure S1c), while the north and south directions accounted for 12% of the data and the intermediate directions accounted for less than 20% of the data. The diurnal wind intensity at 41 and 32 m was on average around 2 and 1.5 m s^{-1} respectively (Figure S1d), and the wind intensity was slightly greater during the night than during daytime, with nearly 1 m s^{-1} more at 41 m and 0.5 m s^{-1} at 32 m. The three lower levels showed very low intensity, below 0.5 m s^{-1}, with only a minor increase during the day.

The friction velocity (u^*) at the two upper levels above the canopy showed a very similar behavior (Figure 1b) but u_* was slightly higher at 32 m (+6%). Diel maxima of u_* of about 0.5 m s^{-1} occurred between 9:00 and 13:00, followed by a prompt decrease of nearly 20% and then a gradual decrease. The minimum (0.13 m s^{-1}) was observed around 20:00, while values between 0.2 and 0.3 m s^{-1} were observed during the night. The in-canopy measurements of friction velocity at the lowest three levels were significantly lower than the above canopy ones: 24 m and 5 m measurements were less than 50% of the two upper levels and 16 m measurements were around 70% less than above canopy levels. The diurnal maxima at noon were 0.25 m s^{-1} at 24 m, 0.18 m s^{-1} at 16 m and 0.26 m s^{-1} at 5 m and during the night the friction velocity showed an almost constant trend with values around 0.1 m s^{-1} at 5 m and around 0.05 m s^{-1} for the two others levels.

3.2 Profiles of temperature, heat fluxes, and atmospheric stability

In the early morning hours after sunrise, the heating of the top part of the canopy developed a thermal inversion in the forest with the ceiling at the top of the canopy (level 24 m) and the base at ground level (Figure 2a).

Above the canopy temperature gradients were strongly super-adiabatic from 4:00 to 17:00, however it should be noted that heat transfer increased significantly only when friction velocity increased.

During the morning, the gradual heating of the canopy reached the upper canopy layer, registering its maximum value at noon. As a consequence, the inversion ceiling was lowered to the bottom part of the tree crowns (16 m). But already from 14:00 the air layers in the middle of the trunk space started to cool and the inversion ceiling gradually reached the top of the canopy again. By 18:00 the top of the canopy had cooled sufficiently for the above-canopy atmosphere to become stable and remain in this condition until 4:00 (Figure 2b).

The presence of an inside canopy thermal inversion is also confirmed by the measured sensible heat fluxes (Figure 3). Above the canopy the heat fluxes were strongly directed upwards during the day. However, the sensible heat fluxes at 32 m were about 20% larger than those at 41 m.

In the upper part of the crown (24 m), sensible heat fluxes were less than half the above canopy ones in the central part of the day. On the contrary, the heat fluxes at 16 m and 5 m were almost always zero or negative (directed downwards). In relation to the strengthening of the thermal inversion in the afternoon, it is worth noting that the downward heat fluxes peaked at 14:00 at 5 m, two hours later at 16 m and four hours later at 24 m.

However, the forest released most of the energy as latent heat showing a peak of about 300 W m^{-2} at midday and presenting very low values in the nighttime.

Above the canopy, the atmosphere was nearly always unstable during the day, while below the canopy it was mostly stable, as shown in Figure 4. At the top canopy level (24 m) the most frequent condition in the central hours of the day was strong instability because of the canopy heating due to radiation. Remarkably, stable conditions at this level strengthened from 15:00 to 19:00 only during the inversion.

Inside the canopy (16 m), the atmosphere was mainly stable or very stable. In particular, from 14:00 to 19:00 the air inside canopy was almost always very stable, as also occurred in the morning from 6:00 to 8:00. During the night, the atmosphere

was mainly stable or very stable above the canopy, while at 24 m and 16 m some nocturnal instability was observed, this instability might be due to numerical artifacts because the sensible heat fluxes were close to zero. A similar explanation can also be used for the stability class distribution at 5 m, for which some instability was observed. In any case, the stable condition was the most frequent situation observed at that level.

3.3 Ozone concentrations profiles

Ozone concentrations above the canopy (41 m and 32 m) showed the typical bell-shaped diurnal pattern, with a maximum around 80 ppb at 14:00 and a minimum around 25 ppb at 4:00 (Figure 5).

The concentrations decreased slightly along the canopy height (-9% between 32 m and 5 m), while there was a significant reduction near the ground (-72% between 32 m and 0.15 m). At ground level, average O_3 concentrations never exceeded 27 ppb. It is worth noting the second (relative) minimum observed at 16:00 at the lowest level; this minimum is in agreement with a slight reduction in the O_3 concentrations observed in the upper levels inside the canopy (from 5 m to 24 m). These features can be better observed considering the vertical variations in Figure S2a and Figure S2b. During the night the in-canopy gradient of O_3 was negligible, but from early morning a negative gradient rapidly developed and remained almost constant (around 0.2 ppb m^{-1}) during the daylight hours, except in the afternoon. The slope of this gradient increased in the afternoon: at 16:00 from 8 m to 32 m (around 0.5 ppb m^{-1}) and at 18:00 but only from 24 m to 32 m (around 0.8 ppb m^{-1}). Another peculiarity emerged from 13:00 to 15:30, when the O_3 concentration just above the canopy (32 m) was on average higher (by 2.0 to 3.8 ppb) than above (41 m); moreover, in the same period, the 24 m O_3 concentration was also higher than the value measured at 41 m (assuming values from 1.2 to 2.5 ppb).

3.4 Ozone fluxes profile

Ozone fluxes were corrected for the storage in the air layers below each measuring point. The magnitude of these corrections was not negligible and they were higher in the morning and the evening (Figure S3) when the air layers in the trunk space are refilling and emptying of O_3, respectively. Considering the whole 41 m height air column, the greatest storage correction was nearly +5 nmol m^{-2} s^{-1} in the morning, while in the evening it was about -4 nmol m^{-2} s^{-1}, the integrated value over the day was null.

Ozone fluxes showed a regular behavior with almost always negative values, except for some positive peaks during the night or during the transition between night and day, in particular in the lowest levels (Figure S4a). The largest deposition flux was observed on the 25th of June at the 24 m with 46 nmol m^{-2} s^{-1} level, which is in agreement with a peak of evapotranspiration (Figure S4b). The following 2 days, O_3 fluxes and LE fluxes were nearly 50% lower.

The good agreement between O_3 fluxes and LE (water) fluxes (Figure S4) suggested the important role of the stomatal activity in the O_3 removal process because stomatal opening can increase both transpiration and O_3 stomatal uptake.

In general, O_3 fluxes and LE fluxes seemed to be correlated, but there were some exceptions (e.g., on the 3rd and 4th of July). The smallest O_3 fluxes were observed on the 6th of July during the rainfall events, after which the O_3 fluxes showed an increase

(7th of July) even if O_3 concentrations were lower. This could be attributed to the enhancement of evapotranspiration fluxes following an increase of soil water content, even though we cannot exclude an influence of the non-stomatal processes (e.g., the increase of NO emissions from soil, Figure 7e).

The average diel course of O_3 fluxes (Figure 6) showed the typical behavior at all levels with low nighttime values and the greatest deposition in the central hours of the day.

Ozone fluxes measured above the canopy (41 m and 32 m) showed very good agreement, nearly overlapped during the day (Figure 6). Both increased very rapidly in the morning and then stayed almost constant (between 8 and 10 nmol m^{-2} s^{-1}) from 9:00 to 16:00, when they started to decrease. At 24 m, fluxes were not constant in the central part of the day, and they were on average 40% greater than the above canopy levels, with average peaks around 15 nmol m^{-2} s^{-1} (Figure 6). From 9:00 to 16:00, air layers above the canopy including the top of the crown (from 24 m to the top of the tower), seemed decoupled from the air below: the above canopy layers were in superadiabatic conditions with intense air mixing (Figure 4a and 4b) while the below canopy layer experienced a thermal inversion that gradually expands towards the top of the canopy and even above after 16:00 (Figure 2b).

The greater fluxes at 24 m might be due to the location of these measurements, which are just in the transient region between well-mixed superadiabatic air and the below canopy thermal inversion.

3.5 NO and NO_2 fluxes and concentrations

NO and NO_2 concentrations along the tower profile (excluding near ground measurements at 0.15 m) were relatively low with maximum values early in the morning of around 2 ppb for NO and around 14 ppb for NO_2. Neither NO nor NO_2 concentrations showed great differences along the vertical profile (Figure 7a and Figure 7b). The greatest differences between the bottom and top level were only around 1 ppb for both compounds, during the early morning hours, between 4:00 and 9:00.

At soil level (0.15 m), the behavior was completely different for both compounds. NO was always greater than the above levels (from 5 m to 41 m) showing two peaks (Figure 7b): the first one around 15 ppb at 6:00 and the second one around 20 ppb at 17:00. NO_2 concentrations at soil level were relatively constant, ranging from 7 to 12 ppb; even in this case two peaks were observed: at 6:00 (10 ppb) and around 17:00 (11 ppb).

NO and NO_2 fluxes at ground level were almost always mono-directional with NO emitted from soil and NO_2 deposited to the ground (Figure 7c). A strong increase in the emission rate of NO and the deposition of NO_2 was observed after the precipitation events occurred between the 6th and the 7th of July (Figure 7d).

The average diel course of soil fluxes showed an almost constant emission of NO and two decreases: the first one around 6:00 and the second one at 17:00. These two decreases in the observed fluxes were strictly linked to the stratification of the air above ground: an increase in the concentrations in a stratified environment led to a reduction of the concentration gradient between soil/litter and the atmosphere thus reducing the emission fluxes. The average diel course of NO_2 deposition was nearly inversely proportional to the behavior of the NO soil fluxes with a pronounced reduction of the deposition early in the morning

and a less intense one in the afternoon. In the afternoon, the nearly simultaneous minimum of soil NO fluxes and maximum of NO_2 deposition (Figure 7e) indicates a gas phase titration with an O_3 reduction due to NO (Figure 5).

At the top of the canopy the net exchange of NO with the above atmosphere was very small, except in the morning, when the deposition peak between 6:00 and 11:00 reached -15 μg N m^{-2} s^{-1} (Figure 7e). This NO deposition (Figure 7e) is correlated to the development of a small NO gradient above the canopy (Figure 7b) after the NO_2 photolysis. The NO gradient and fluxes became negligible (Figure 7b and Figure 7e) when the NO_2 concentrations reached a minimum (Figure 7a) determined by the photolytic equilibrium of NO_x.

4 Discussion

While turbulence and heat fluxes inside tree canopies have been extensively investigated, only a few studies had attempted to partition O_3 fluxes using flux measurements at different in-canopy heights (Dorsey et al., 2004; Launiainen et al., 2013).

The evaluation of flux profiles relies on the constant flux hypothesis, one of the fundamental theories of micrometeorology (Arya, 2001). In the case of the Bosco Fontana measurements, it was expected that the fluxes measured at 41 m and 32 m were almost equal because both heights are above the forest canopy level, and that the deposition flux should decrease, in absolute terms, at the lower levels due to the presence of different in-canopy sinks for O_3 (stomata and surfaces of the leaves, branches, and stems). However, although O_3 fluxes were similar at the two above-canopy heights (41 m and 32 m) and within the uncertainty of the measurement, during the morning hours O_3 deposition at 24 m was significantly higher than at the two upper levels (32 m and 41 m). Actually, between 9:00 and 12:00, O_3 fluxes at 24 m were on average nearly 3 nmol m^{-2} s^{-1} higher than above the canopy (Figure 6), while they were nearly equal between 13:00 and 18:00 (fluxes at 24 m were only 0.5 nmol m^{-2} s^{-1} higher).

A possible explanation of the higher O_3 fluxes at 24 m could lie in the different footprints of the eddy covariance measurements coupled with the heterogeneity of the canopy (Dalponte et al., 2007; Acton et al., 2016). The footprints of the measurements at 41 m, 32 m and 24 m all fell inside the surface of the upper forest canopy, even though the 24 m level was just at the top canopy edge. The size of the footprint areas decreased at decreasing measuring heights. However, without any source or sink of the considered scalar, the horizontal homogeneity of the studied ecosystem ensures the validity of the constant flux hypothesis and thus the measurements referred to different footprints should be the same, i.e., fluxes with larger footprints (measurements at 41 m and 32 m) should be comparable to those with smaller footprints (measurements at 24 m).

Regarding a possible role of BVOCs emission on the O_3 deposition fluxes, a partition exercise showed that less than 3% of the O_3 deposited to the Bosco Fontana forest was destroyed by reactions with isoprene (Nemitz 2013, personal communication), which was the most emitted BVOC at the site (Schallahart et al., 2016). The reaction of O_3 with isoprene was estimated from the methylvinylketone (MVK)/methacrolein (MACR) flux measured above the canopy by Schallahart et al. (2016) by means of a PTR-ToF spectrometer (71 atomic mass units), and by neglecting the fact that MVK/MACR can also be directly exchanged with the vegetation and produced by the competing isoprene vs. OH reaction. This result suggests a minor influence of the

BVOCs emission on the enhancement of the O_3 fluxes observed at the top of the canopy (24 m) in the morning. However, we cannot exclude that fast reactions between O_3 and undetected highly-reactive BVOCs occurred, e.g. with isoprenoids emitted at the canopy level such as the β-Caryophillene, a sesquiterpene which reacts in the gas phase in few seconds to produce both unidentified oxidized VOCs and SOA, as highlighted by Goldstein et al. (2004).

To investigate alternative reasons for the enhancement of the O_3 fluxes at 24 m a spectral analysis was performed to compare the normalized cospectra of the O_3 fluxes at the different levels, and the role of the NO-related O_3 chemical sink was analyzed. Figure S5 shows the average normalized cospectra of the vertical component of wind and O_3 for the measurements performed when the morning O_3 enhancement at 24 m occurred (11:00) and when the 24 m O_3 fluxes were comparable with the upper ones (15:00). The cospectra analysis did not provide an obvious explanation for the enhancement of the fluxes observed at 24 m in the morning. Apart from the O_3 cospectra at 16 m which had a very irregular behavior, the other three cospectra did not show any particular difference, which could explain the higher O_3 fluxes at 24 m. The observed decrease of the O_3 cospectra at 24 m and 16m for frequency above 0.1 Hz is consistent with the notion that within the canopy the mean eddy-size is dictated by the canopy height.

The analysis of the NO-related chemical sink revealed a possible role of the convergence of two NO fluxes at the top of the canopy (i.e., the NO deposition flux from the air above the forest and the soil NO emission flux uprising from the forest floor) on the enhancement of the O_3 fluxes at 24 m. This can be argued by considering the differences between the O_3 fluxes measured at 24 m and those measured at 32 m (a level where the constant flux hypothesis is confirmed). The sum of these differences from 6:00 to 12:00 gives a value of 59.4 μmol O_3 m^{-2}, which is almost equal to the sum of the NO converging to the top of the canopy, both from above and below in the same hours (54 μmol NO m^{-2}).

Assuming a stoichiometric reaction between NO and O_3 at the top of the canopy, the part of the O_3 flux not due to this chemical sink is obtained by subtracting to the 24 m O_3 fluxes value an amount of O_3 equal to the NO converging at the top of the canopy during each half hour. This is shown in Figure 8, where the measured O_3 flux at 24 m is represented as a green line and the resulting part of the O_3 flux at 24 m not due to the NO-related sink is reported as a dark grey dashed line, while the NO fluxes converging from above and below canopy are represented by the black and purple lines, respectively.

The good agreement during the daylight hours between the O_3 fluxes at 32 m (Figure 8, red line) and the part of the O_3 flux at 24 m not due to the NO-related sink (Figure 8, dark grey dashed line) suggests that the enhancement of the O_3 fluxes observed at 24 m was related to the interactions between O_3 and NO at the top canopy level. However, at night there might be an overcorrection of the O_3 flux at 24 m (Figure 8) because, in case of high atmospheric stability, the NO emitted from soil could stratify near the forest floor and react below the canopy.

The coupling between the forest and the atmosphere above the canopy was found to have an important role on the regulation of the O_3 flux enhancement at 24 m, facilitating this mechanism particularly during the morning hours when the in-canopy mixing processes were well developed. In fact, the decrease of the soil level NO concentrations (Figure 7b) from 6:00 to 12:00 suggests a relatively well-mixed forest canopy, which is better coupled with the atmosphere above. This condition also allowed O_3 and NO from the above canopy air to penetrate more easily into the canopy (see Figure S2b and the morning peak of Figure

7b). On the contrary, the increase of the NO concentrations at soil level (0.15 m, Figure 7b) after midday, followed by the decrease of O_3 concentrations at the same level (Figure 5), suggests that an air stratification occurred inside the canopy in the afternoon with a decoupling from the above canopy air, as also found by Rummel et al., (2002) and Foken (2008). The afternoon stratification was also supported by the stability classes reported in Figure 4c and Figure 4d which denoted almost always stable or very stable atmospheric conditions both at 16 m and 24 m from 15:00 to 18:00. In addition, the thermal inversion layer within the canopy increased its thickness during the afternoon (Figure 2b) rising from 16 m (around 12:00) to 24 m (between 14:00 and 16:00). Again, the morning coupling and the afternoon decoupling was supported by the diurnal course of the specific humidity observed below the canopy (Figure 1a). In the morning the almost constant amount of water vapour above and below canopy (other than the 24 m level where there was an unidentified process removing water vapour) reveals an efficient mixing of the air, while in the afternoon, the increase of the specific humidity from the three lower levels, due to soil evaporation and understorey transpiration, reveals an air stratification below canopy and a forest decoupling from the above atmosphere.

The availability of O_3 flux measurements at different heights within and above the canopy allowed a partition of the O_3 fluxes among the different ecosystem layers: upper and lower canopy, understorey and soil. To do that we assumed the O_3 flux measured at 32 m as the total deposition flux, and then calculated the overall NO sink as the sum of the NO deposited from the above atmosphere and the NO emitted from the soil, considering a stoichiometric reaction between NO and O_3. The O_3 uptake due to the upper canopy layer was identified as the difference between the O_3 fluxes measured at 32 m and those measured at 16 m (ignoring the apparently enhanced values at 24 m), while the O_3 uptake due to the lower canopy layer was obtained as the difference between the O_3 fluxes measured at 16 m and 5 m. Finally, the deposition to the forest floor (soil and the understorey vegetation) was calculated as the difference between the O_3 flux at 5 m and the NO flux emitted from the soil, namely the amount of O_3, which is not removed by chemical reaction with NO.

The result of this test is shown in Figure 9, where it can be observed that on a daily basis the upper canopy layer of the forest removed about 1/3 of the total deposited O_3 (between 7:00 and 22:00) while the lower canopy layer of the forest removed the main part of the O_3 (46.5%, between 8:00 and 2200).

The canopy removed nearly 80% of the O_3 deposited to the forest ecosystem, but it is worth noticing that this amount included stomatal uptake and non-stomatal processes such as dry deposition on physical surfaces (e.g., leaves and bark) and chemical reactions in ambient air. Only a minor part of O_3 was removed by the understorey vegetation or deposited to the soil (2.0%), while an important role was played by the NO-related sink, mainly due to soil emissions, which accounted for 18.2% of the total O_3 deposition.

This latter result is in agreement with the observations of Dorsey et al., (2004) who found that in a Douglas fir plantation, between 7% and 14% of the O_3 deposition in the daylight hours could be attributed to reactions with the NO emitted from soil, while this fraction increased up to 41% during the night. Similarly, Pilegaard (2001) found that the NO sink accounted for a 25% of the O_3 deposition in a Norway spruce forest, with an increase of this fraction up to 31% during the night.

Nearly all of the nighttime O_3 deposition at Bosco Fontana can be attributed to O_3 depletion due to NO. The fact that NO reaction accounts for 100% of the nocturnal O_3 deposition would imply that other non-stomatal sinks are negligible during that time. However, it cannot be excluded that some non-stomatal deposition of O_3 took place since our stirred soil flux chambers could somewhat overestimate the nocturnal soil NO emission, due to the enhanced amount of mixing in the flux chamber compared with the true forest floor during calm nights. Similarly, the analysis assumes that the only sink for NO is its reaction with O_3. A small NO uptake by vegetation is possible even if unlikely as shown by Teklemariam et al., (2006) and Stella et al. (2013). Overall this ecosystem did not behave as a net NO emitter because the whole NO produced at soil level is consumed within the canopy, but as a weak NO sink because of the small amount of NO received from the atmosphere in the first hours of the morning (Figure 7d). This differs from the observation of Dorsey et al. (2004) who estimated that nearly 60% of the NO emitted from the soil of a Douglas Fir forest escaped the trunk space to react aloft.

5 Conclusions

Ozone flux measurements were carried out at five levels (above, inside, and below the canopy) along a vertical profile of a mature broadleaf forest during the ECLAIRE joint field campaign. The data collected are particularly relevant since no measurements of O_3 fluxes were previously available in the literature for an oak-hornbeam mature forest. Ozone fluxes measured at the two levels above the canopy were in good agreement and comparable to those reported for other forest types (Amthor et al., 1994; Gerosa et al., 2005; Hogg et al., 2007; Rummel et al., 2007; Finco et al., 2017). Ozone fluxes at 16 m and 5 m were lower than above the canopy, while at the top canopy edge (24 m) fluxes were surprisingly higher than above in the morning hours. The main cause of this enhancement was attributed to a chemical O_3 sink due to a reaction between O_3 and NO, which was emitted from the soil and deposited from the atmosphere above the canopy.

The morning enhancement of the O_3 fluxes at 24 m was favored by the coupling between the forest and the atmosphere, while in the afternoon the decoupling and the in-canopy stratification led to 24 m fluxes comparable to those above the canopy.

Most of the O_3, nearly 80%, was removed by the forest canopy through stomatal uptake, dry deposition on physical surfaces and ambient chemistry: in particular, the upper canopy layer removed 33.3% of the O_3 deposited and the lower canopy layer 46.3%. Only a minor part of O_3 was deposited on the soil and the understorey (2%), while the remaining part (18.2%) was removed by a chemical reaction with NO emitted from soil. These findings might be useful for improving the O_3 risk assessment for mature forests.

The collected data will be available for the parameterization and the fine-tuning of process models aimed at correctly reproducing the in-canopy dynamics of the reactions between O_3 and NO_x, as these dynamics might significantly influence the biosphere-atmosphere exchange budgets of O_3 and other reactive trace compounds with further implications for air quality and productivity of the forest ecosystems.

Acknowledgements. The authors are grateful to the administration and the personnel of the Bosco Fontana National Reserve for their availability and continuous support, to the European Union for having fund the project ECLAIRE under which this campaign was performed.

This publication was funded by the Catholic University of the Sacred Heart in the frame of its Programs of promotion and dissemination of the scientific research.

References

- Acton, W. J. F., Schallhart, S., Langford, B., Valach, A., Rantala, P., Fares, S., Carriero, G., Tillmann, R., Tomlinson, S. J., Dragosits, U., Gianelle, D., Hewitt, C. N., and Nemitz, E.: Canopyscale flux measurements and bottom-up emission estimates of volatile organic compounds from a mixed oak and hornbeam forest in northern Italy, Atmos. Chem. Phys., 16, 7149–7170, doi:10.5194/acp-16-7149-2016, 2016.
- Altimir, N., Tuovinen, J.-P., Vesala, T., Kulmala, M., and Hari, P.: Measurements of ozone removal to Scots pine shoots: calibration of a stomatal uptake model including the non-stomatal component, Atmos. Environ., 38, 2387–2398, 2004.
- Altimir, N., Kolari, P., Tuovinen, J.-P., Vesala, T., Back, J., Suni, T., Kulmala, M., and Hari, P.: Foliage surface ozone deposition: a role for surface moisture?, Biogeosciences, 3, 209-228, doi: http://www.biogeosciences.net/3/209/2006/, 2006.
- Arya, S. P.: Introduction to Micrometeorology, Academic Press, San Diego, USA, pp 415, 2001.
- Amthor, J. S., Goulden, M. L., Munger, J. W., and Wofsy, S.C.: Testing a mechanistic model of forest-canopy mass and energy exchange using eddy correlation: carbon dioxide and ozone uptake by a mixed oak-maple stand, Func. Plant Biol., 21, 623-651, 1994.
- Aubinet, M., Grelle, A., Ibrom, A., Rannik, U., Moncrieff, J., Foken, T., Kowalski, A. S., Martin, P. H., Berbigier, P., Bernhofer, C., Clement, R., Elbers, J., Granier, A., Grunwald, T., Morgenstern, K., Pilegaard, K., Rebmann, C., Snijders, W., Valentini, R., and Vesala, T.: Estimates of the annual net carbon and water exchange of forests: The EUROFLUX methodology, Adv. Ecol. Res., 30, 113–175, 2000.
- Aubinet, M., Chermanne, B., Vandenhaute, M., Longdoz, B., Yernaux, M. and Laitat, E.: Long term carbon dioxide exchange above a mixed forest in the Belgian Ardennes, Agric. For. Meteorol, 108, 293–315, 2001.
- Aubinet, M., Vesala, T., Papale, D. (Eds): Eddy Covariance. A practical guide to measurement and data analysis. Springer, Netherlands, 2012.
- Bauer, M. R., Hultman, N. E., Panek, J. A., and Goldstein, A. H.: Ozone deposition to a ponderosa pine plantation in the Sierra Nevada Mountains (CA): A comparison of two different climatic years, J. Geophys. Res.- Atmos., 105, 22123–22136, 2000.
- Bellumè M., Maugeri M., and Mazzucchelli E.: Due secoli di osservazioni meteorologiche a Mantova, Edizioni CUSL, Milano (Italy), pp. 124, 1998.
- Büker, P., Morrissey, T., Briolat, A., Falk, R., Simpson, D., Tuovinen, J.-P., Alonso, R., Barth, S., Baumgarten, M., Grulke, N., Karlsson, P.E., King, J., Lagergren, F., Matyssek, R., Nunn, A., Ogaya, R., Peñuelas, J., Rhea, L., Schaub,

M., Uddling, J., Werner, W. and Emberson, L.D.: DO3SE modelling of soil moisture to determine ozone flux to European forest trees, Atmos. Chem. Phys. 12, 5537–5562, 2012.

- Butterbach-Bahl K., Gasche R., Breuer L., and Papen H.: Fluxes of NO and N_2O from temperate forest soils: impact of forest type, N deposition and of liming on the NO and N_2O emissions, Nutr. Cycl. Agroecosyst. 48, 79-90, 1997.
- Campanaro A., Hardersen S., and Mason F.: Piano di Gestione della Riserva Naturale e Sito Natura 2000 "Bosco della Fontana". Quaderni Conservazione Habitat, 4. Cierre Edizioni, Verona (Italy), pp. 221, 2007.
- Cape J.N., Hamilton R., and Heal M.R.: Reactive uptake of ozone at simulated leaf surfaces: implications for 'non-stomatal'ozone flux. Atmos. Environ, 43, 1116-1123, 2009.
- Cieslik S.: Energy and ozone fluxes in the atmospheric surface layer observed in Southern Germany highlands, Atmos. Environ., 32, 1273-1281, 1998.
- Clifton O.E., Fiore A.M., Munger J.W., Malyshev S., Horowitz L.W., Shevliakova E., Paulot F., Murray L.T., Griffin K.L.: Interannual variability in ozone removal by a temperate deciduous forest. Geophys. Res. Let., 44, 542-552, 2017.
- Coe, H., Gallagher, M. W., Choularton, T. W., and Dore, C.: Canopy Scale Measurements Of Stomatal And Cuticular O3 Uptake By Sitka Spruce, Atmos. Environ., 29, 1413–1423, 1995.
- Dalponte M., Giannelle D., and Bruzzone L.: Use of hyperspectral and LIDAR data for classification of complex forest areas. In: Gianelle D, Travaglini D, Mason F, Minari E, Chirici G, Chemini C (eds.) Canopy analysis and dynamics of a floodplain forest. Rapporti scientifici, 3, Cierre Grafica Editore, Verona, pp 25–37, 2007.
- Dorsey, J.R., Duyzer, J.H., Gallagher, M.W., Coe, H., Pilegaard, K., Weststrate, J.H.,Jensen, N.O., Walton, S.: Oxidized nitrogen and ozone interaction with forests. I: Experimental observations and analysis of exchange with Douglas fir, Q. J. Roy. Meteor. Soc., 130, 1941–1955, 2004.
- Emberson, L.D., Ashmore, M.R., Cambridge, H.M., Simpson, D., and Tuovinen, J.-P.: Modelling stomatal ozone flux across Europe, Environ. Pollut., 109, 3, 403-413, 2000.
- Ermel M., Oswald R., Mayer J.-C., Moravek A., Song G., Beck M., Meixner F. X., and Trebs I.: Preparation methods to optimize the performance of sensor discs for fast chemiluminescence ozone analyzers, Environ. Sci. Technol. 47, 1930-2936, 2013.
- Fares, S., Park, J.-H., Ormeno, E., Gentner, D. R., McKay, M., Loreto, F., Karlik, J., and Goldstein, A. H.: Ozone uptake by citrus trees exposed to a range of ozone concentrations, Atmos. Environ., 44, 3404–3412, doi:10.1016/j.atmosenv.2010.06.010, 2010.
- Fares, S., Weber, R., Park, J.-H., Gentner, D., Karlik, J., and Goldstein, A. H.: Ozone deposition to an orange orchard: Partitioning between stomatal and non-stomatal sinks, Environ. Pollut., 169, 258–266, doi:10.1016/j.envpol.2012.01.030, 2012

- Fares, S., F. Savi, A., Muller, J.B.A., Matteucci, G., Paoletti, E.: Simultaneous measurements of above and below canopy ozone fluxes help partitioning ozone deposition between its various sinks in a Mediterranean Oak Forest, Agr. Forest Meteorol. 198–199, 181–191, 2014.
- Finco, A., Marzuoli, R., Chiesa, M., and Gerosa. G.: Ozone risk assessment for an Alpine larch forest in two vegetative seasons with different approaches: comparison of POD1 and AOT40, Environ. Science and Poll. Res, 24 (34):26238-26248, 2017.
- Foken T. and Wichura B.: Tools for quality assessment of surface-based flux measurements, Agr. Forest Meteorol.,78, 83-205, 1996.
- Foken, T.: Micrometeorology, Springer-Verlag, Berlin Heidelberg, Germany, 2008.
- Foken, T., Meixner, F. X., Falge, E., Zetzsch, C., Serafimovich, A., Bargsten, A., Behrendt, T., Biermann, T., Breuninger, C., Dix, S., Gerken, T., Hunner, M., Lehmann-Pape, L., Hens, K., Jocher, G., Kesselmeier, J., Lüers, J., Mayer, J.-C., Moravek, A., Plake, D., Riederer, M., Rütz, F., Scheibe, M., Siebicke, L., Sörgel, M., Staudt, K., Trebs, I., Tsokankunku, A., Welling, M., Wolff, V., and Zhu, Z.: Coupling processes and exchange of energy and reactive and non-reactive trace gases at a forest site – results of the EGER experiment, Atmos. Chem. Phys., 12, 1923-1950, 2012.
- Fontan, J., Minga, A., Lopez, A. and Druilhet, A.: Vertical ozone profiles in a pine forest. Atmos. Environ. 26, 863–869, 1992.
- Fowler, D., Pilegaard, K., Sutton, M.A., Ambus, P., Raivonen, M., Duyzer, J., Simpson, D., Fagerli, H., Sandro Fuzzi, Schjoerring, J.K., Granier, C., Neftel, A., Isaksen, I.S.A., Laj, P., Maione, M., Monks, P.S., Burkhardt, J., Daemmgen, U., Neirynck, J., Personne, E., Wichink-Kruit, R., Butterbach-Bahl, K., Flechard, C., Tuovinen, J.P., Coyle, M., Gerosa, G., Loubet, B., Altimir, N., Gruenhage, L., Ammann, C., Cieslik, S., Paoletti, E., Mikkelsen, T.N., Ro-Poulsen, H., Cellier, P., Cape, J.N., Horváth, L., Loreto, F., Niinemets, U., Palmer, P.I., Rinne, J., Misztal, P., Nemitz, E., Nilsson, D., Pryor, S., Gallagher, M.W., Vesala, T., Skiba, U., Brüggemann, N., Zechmeister-Boltenstern, S., Williams, J., O'Dowd, C., M.C. Facchini, de Leeuw, G., Flossman, A., Chaumerliac, N., and Erisman, J.W.: Atmospheric Composition Change: Ecosystems – Atmosphere interactions, Atmos. Environ., 43, 5193-5267, 2009.
- Fuentes, J. D., Gillespie, T. J., Denhartog, G., and Neumann, H. H.: Ozone Deposition onto a Deciduous Forest During Dry and Wet Conditions, Agr. Forest Meteorol., 62, 1–18, 1992.
- Ganzeveld, L., Lelieveld, J., Dentener, F. J., Krol, M. C., Bouwman, A. F., and Roelofs, G. J.: The influence of soil-biogenic NOx emissions on the global distribution of reactive trace gases: the role of canopy processes, J. Geophys. Res., 107, https://doi.org/10.1029/2001JD001289, 2002
- Ganzeveld, L., Ammann, C.. and Loubet, B.: Modelling Atmosphere-Biosphere Exchange of Ozone and Nitrogen Oxides, in R.-S. Massad and B. Loubet (eds.), Review and Integration of Biosphere-Atmosphere Modelling of Reactive Trace Gases and Volatile Aerosols, 85-105, 2015.

- Gasche R., and Papen H.: A 3-year continuous record of nitrogen trace gas fluxes from untreated and limed soil of a N-saturated spruce and beech forest ecosystem in Germany. 2. NO and NO_2 fluxes, J. Geophys. Res. 104, 18505-28520, 1999.
- Gerosa, G., Fusaro, L., Monga, R., Finco, A., Fares, S., Manes, F. and Marzuoli, R.:. A flux-based assessment of above and below ground biomass of Holm oak (*Quercus ilex* L.) seedlings after one season of exposure to high ozone concentrations, Atmospheric Environment 113, 41-49, 2015.
- Gerosa, G., Marzuoli, R., Monteleone, B., Chiesa, M. and Finco, A.: Vertical ozone gradients above forests. Comparison of different calculation options with direct ozone measurements above a mature forest and consequences for ozone risk assessment, Forests, 8, 337, 2017.
- Gerosa, G., Vitale, M., Finco, A., Manes, F., Ballarin-Denti, A., and Cieslik, S.: Ozone uptake by an evergreen Mediterranean forest (*Quercus ilex*) in Italy. Part I: micrometeorological flux measurements and flux partitioning, Atmos. Environ. 39, 3255-3266, 2005.
- Gerosa, G., Finco, A., Mereu, S., Vitale, M., Manes, F., Ballarin-Denti, A.: Comparison of seasonal variations of ozone exposure and fluxes in a Mediterranean Holm oak forest between the exceptionally dry 2003 and the following year, Environ. Pollut. 157, 1737–1744, 2009a.
- Gerosa, G., Finco, A., Mereu, S., Marzuoli, R., and Ballarin-Denti, A.: Interactions among vegetation and ozone, water and nitrogen fluxes in a coastal Mediterranean maquis ecosystem, Biogeosciences 6, 1783-1798, 2009b.
- Goldstein, A. H., McKay, M., Kurpius, M. R., Schade, G. W., Lee, A., Holzinger, R., and Rasmussen, R. A.: Forest thinning experiment confirms ozone deposition to forest canopy is dominated by reaction with biogenic VOCs, Geophys. Res. Lett., 31, L22106, doi: 10.1029/2004GL21259, 2004.
- Güsten H., and Heinrich G.: On-line measurements of ozone surface fluxes: Part I. Methodology and instrumentation, Atmos. Environ. 6, 897-909, 1996.
- Hogg, A., Uddling, J., Ellsworth, D., Carroll, M. A., Pressley, S., Lamb, B., and Vogel, C.: Stomatal and non-stomatal fluxes of ozone to a northern mixed hardwood forest, Tellus B, 59, 514– 525, 2007.
- Horvath, L., Nagy, Z. and Weidinger, T.,: Estimation of dry deposition velocities of nitric oxide, sulfur dioxide, and ozone by the gradient method above short vegetation during the TRACT campaign, Atm. Env., 32, 7, 1317-1322, 1998.
- Jarvis P.G.: The interpretation of the variations in leaf water potential and stomatal conductance found in canopies in the field, Philos. T. Roy. Soc. B., 273, 593–610, 1976.
- Keronen, P., Reissell, A., Rannik, U., Pohja, T., Siivola, E., Hiltunen, V., Hari, P., Kulmala, M., and Vesala, T.: Ozone flux measurements over a Scots pine forest using eddy covariance 25 method: performance evaluation and comparison with flux-profile method, Boreal Environ. Res., 8, 425–444, 2003.

- Kramm, G., Muller, H., Fowler, D., Hofken, K.D., Meixner, F. X. and Schaller, E,. A modified profile method for determining the vertical fluxes of NO, NO2, Ozone and HNO3 in the atmospheric surface layer. Journ. of Atm. Chem., 13 (3). 265-288.
- Lamaud, E., Carrara, A., Brunet, Y., Lopez, A., and Druilhet, A.: Ozone fluxes above and within a pine forest canopy in dry and wet conditions, Atmos. Environ., 36, 77–88, 2002.
- Langford, B., Acton, W., Ammann, C., Valach, A., and Nemitz, E.: Eddy-covariance data with low signal-to-noise ratio: time-lag determination, uncertainties and limit of detection, Atmos. Meas. Tech. 8, 4197-4213, 2015.
- Launiainen, S., Katul, G.G., Gronholm, T., and Vesala, T.: Partitioning ozone fluxes between canopy and forest floor by measurements and a multi-layer model, Agr. Forest Meteorol. 173, 85–99, 2013.
- Lee X., Massman W., and Law B.: Handbook of Micrometeorology: A Guide for Surface Flux Measurements and Analysis, Kluwer Academic Publisher, Dordrecht, 2004.
- Longo L.: Clima. In: Mason F. (ed.). Dinamica di una foresta della Pianura Padana. Bosco della Fontana. Seconda edizione con Linee di gestione forestale. Rapporti Scientifici 1. Centro Nazionale Biodiversità Forestale Verona - Bosco della Fontana. Arcari Editore, Mantova (Italy), pp. 16-27, 2004.
- Marzuoli, R., Bussotti, F., Calatayud, V., Calvo, E., Alonso, R., Bermejo, V., Pollastrini, M., Monga, R. and Gerosa, G.: Dose-response relationships for ozone effect on the growth of deciduous broadleaf oaks in mediterranean environment, Atmos. Env., 190, 331-341.
- Matyssek, R., Wieser, G., Calfapietra, C., de Vries, W., Dizengremel, P., Ernst, D., Jolivet, Y., Mikkelsen, T.T., Mohren, G.M.J., Le Thiec, D., Tuovinen, J.P., Weatherall, A., and Paoletti, E.: Forests under climate change and air pollution: gaps in understanding and future directions for research, Environ. Pollut. 160, 57–65, 2012.
- McMillen, R.T.: An Eddy Correlation Technique with Extended Applicability to Non-Simple Terrain, Boundary-Lay Meteorol. 43, 231–245, 1988.
- Mikkelsen, T. N., Ro-Poulsen, H., Pilegaard, K., Hovmand, M. F., Jensen, N. O., Christensen, C. S., and Hummelshoej, P.: Ozone uptake by an evergreen forest canopy: temporal variation and possible mechanisms, Environ. Pollut., 109, 423–429, 2000.
- Mikkelsen, T. N., Ro-Poulsen, H., Hovmand, M. F., Jensen, N.O., Pilegaard, K. and Egeløv, A. H.: Five-year measurements of ozone fluxes to a Danish Norway spruce canopy, Atmos. Environ. 38, 2361-2371, 2004.
- Muller, J. B. A., Percival, C. J., Gallagher, M. W., Fowler, D., Coyle, M. and Nemitz, E.: Sources of uncertainty in eddy covariance ozone flux measurements made by dry chemiluminescence fast response analysers, Atmos. Meas. Tech., 3, 163-176, 2010.
- Padro J.: Summary of ozone dry deposition velocity measurements and model estimates over vineyard, cotton, grass and deciduous forest in summer, Atmos. Environ., 30, 2363-2369, 1996.
- Pilegaard, K.: Air–soil exchange of NO, NO_2 and O_3 in forests, Water, Air, and Soil Poll.: Focus 1, 79–88, 2001.

- Rannik, Ü., Altimir, N., Mammarella, I., Bäck, J., Rinne, J., Ruuskanen, T. M., Hari, P., Vesala, T., and Kulmala, M.: Ozone deposition into a boreal forest over a decade of observations: evaluating deposition partitioning and driving variables, Atmos. Chem. Phys., 12, 12165-22182, https://doi.org/10.5194/acp-22-22165-2012, 2012.
- Rosenkranz, P., Brüggemann, N., Papen, H., Xu, Z., Seufert, G., and Butterbach-Bahl, K.: N_2O, NO and CH_4 exchange, and microbial N turnover over a Mediterranean pine forest soil, Biogeosciences 3, 121-133, 2006.
- Rummel, U., Ammann, C., Gut, A., Meixner, F. X., and Andreae, M. O.,. Eddy covariance measurements of nitric oxide flux within an Amazonian rainforest, J. Geophys. Res. Atm.: 107, D20, 17, 1-9, 2002.
- Rummel, U., Ammann, C., Kirkman, G. A., Moura, M. A. L., Foken, T., Andreae, M. O., and Meixner, F. X.: Seasonal variation of ozone deposition to a tropical rain forest in southwest Amazonia, Atmos. Chem. Phys. 7, 5415–5435, 2007.
- Schallhart, S., Rantala, P., Nemitz, E., Taipale, D., Tillmann, R., Mentel, T. F., Loubet, B., Gerosa, G., Finco, A., Rinne, J., and Ruuskanen, T. M.: Characterization of total ecosystem-scale biogenic VOC exchange at a Mediterranean oak–hornbeam forest, Atmos. Chem. Phys. 16, 7171-7194, 2016.
- Schotanus, P., Nieuwstadt, F., and De Bruin, H. A. R.: Temperature measurement with a sonic anemometer and its application to heat and moisture fluxes, Boundary-Lay. Meteorol.26, 81-93, 1983.
- Stella, P., Loubet, B., Lamaud, E., Laville, P., and Cellier, P.: Ozone deposition onto bare soil: a new parameterisation, Agr. Forest Meteorol., 151, 669–681, 2011.
- Stella, P., Kortner, M., Ammann, C., Foken, T., Meixner, F. X., and Trebs, I.: Measurements of nitrogen oxides and ozone fluxes by eddy covariance at a meadow: evidence for an internal leaf resistance to NO_2, Biogeosciences, 10, 5997-6017, 2013.
- Teklemariam, T. A. and Sparks, J. P.: Leaf fluxes of NO and NO2 in four herbaceous plant species: The role of ascorbic acid, Atmos. Environ., 40, 2235-2244, 2006.
- Utiyama, M., Fukuyama, T., Maruo, Y.Y., Ichino, T., Izumi, K., Hara, H., Takano, K.,Suzuki, H., Aoki, M.: Formation and deposition of ozone in a red pine forest. Water, air, and soil poll. 151, 53–70. 2004
- Vickers D. and Mahrt L.: Quality Control and Flux Sampling Problems for Tower and Aircraft Data, J. Atmos. Oceanic Technol., 14, 512–526, 1997.
- Walton, S., Gallagher, M. W. and Duyzer, J. H: Use of a detailed model to study the exchange od NOx and O_3 above and below a deciduous canopy. Atmos. Environ., 31, 2915–2931, 1997.
- Webb, E. K., Pearman, G. I., and Leuning, R.: Correction of flux measurements for density effects due to heat and water vapour transfer, Q. J. Roy. Meteor. Soc. 106, 85–100, 1980.
- Wilczak J. M., Oncley S. P., Sage,S. A.: Sonic anemometer tilt correction algorithms, Boundary-Lay. Meteorol. 99, 127-150, 2001.

- Wittig, V.E., Ainsworth, E.A., Naidu, S.L., Karnosky, D.F., Long, S.P., 2009. Quantifying the impact of current and future tropospheric ozone on tree biomass, growth, physiology and biochemistry: a quantitative meta-analysis, Global Change Biol. 15, 396–424.
- Wu X., Brüggemann N., Gasche R., Shen Z., Wolf B., and Butterbach-Bahl K.: Environmental controls over soil-atmosphere exchange of N_2O, NO, and CO_2 in a temperate Norway spruce forest, Global Biogeochem. Cy. 24, 2, 2010.
- Zona, D., Gioli, B., Fares, S., De Groote, T., Pilegaard, K., Ibrom, A., and Ceulemans, T.: Environmental controls on ozone fluxes in a poplar plantation in Western Europe, Environ. Pollut., 184, 201-210, 2014.

Table 1 - Instruments installed at each level of the tower and on the mast at 5 m a.g.l. In brackets are indicated the variable measured by each instrument and the manufacturer. (T is air temperature, RH is relative humidity, NR is net radiation, P is pressure, Rain is precipitation, SWC is soil water content, SHF is soil heat flux). The soil dynamic chamber system is described in the methodological part.

Level / Height (m)	Ultrasonic anemometers	Fast O_3 analyzers	Other fast analyzers	Slow sensors	
41	USA1 (*Metek, D*)	COFA (*Ecometrics, I*)	LI-COR 7500 (CO_2, H_2O, *Li-Cor, USA*)	HMP45 NR-lite BF5 PTB101B Rain gauge 52202	(T, RH, *Vaisala, FIN*) (NR, *Kipp & Zonen, NL*) (PAR,*Delta-T Devices, UK*) (P, *Vaisala, FIN*) (Rain, *Campbell Scientific, USA*)
32	HS50 (*Gill, UK*)	ROFI (*CEH, UK*)	CLD780TR (NO, *Ecophysics, CH*)	HMP45	(T, RH, *Vaisala, FIN*)
24	Windmaster PRO (*Gill, UK*)	FROM (*NOAA, USA*)	-	HMP45	(T, RH, *Vaisala, FIN*)
16	Windmaster PRO (*Gill, UK*)	COFA (*Ecometrics, I*)	-	HMP45	(T, RH, *Vaisala, FIN*)
11	-	-	-	HMP45	(T, RH, *Vaisala, FIN*)
5	R2 (*Gill, UK*)	FOS (*Sextant, NZ*)	LI-COR 7500 (CO_2, *Li-Cor, USA*)		-
1.5	-	-	-	PT100	(T, *Campbell Scientific, USA*)
0.15	-	-	-	PT100	(T, *Campbell Scientific, USA*)
Soil	-	-	-	TDR mod 616 HFP01SC PT100 Soil dynamic chamber system (*IMK-IFU, D*)	(SWC, *Campbell Scientific, USA*) (SHF, *Hukseflux, NL*) (T, *GMR Strumenti, I*)

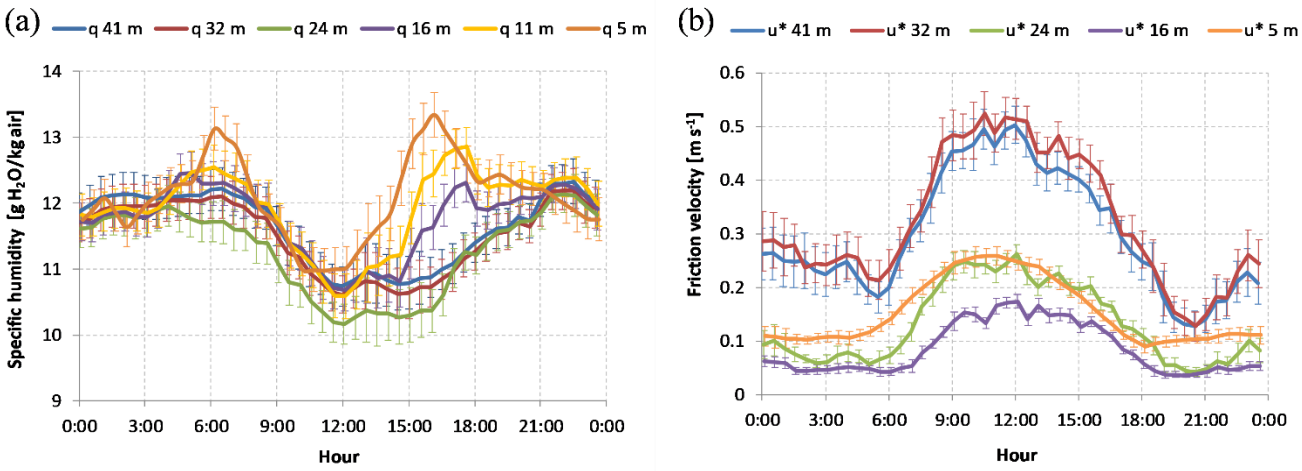

Figure 1 – (a) Average diel course of specific humidity (q) at the five levels; (b) average diel course of friction velocity (*u) at the five levels.). Vertical bars represent the standard error of the mean.**

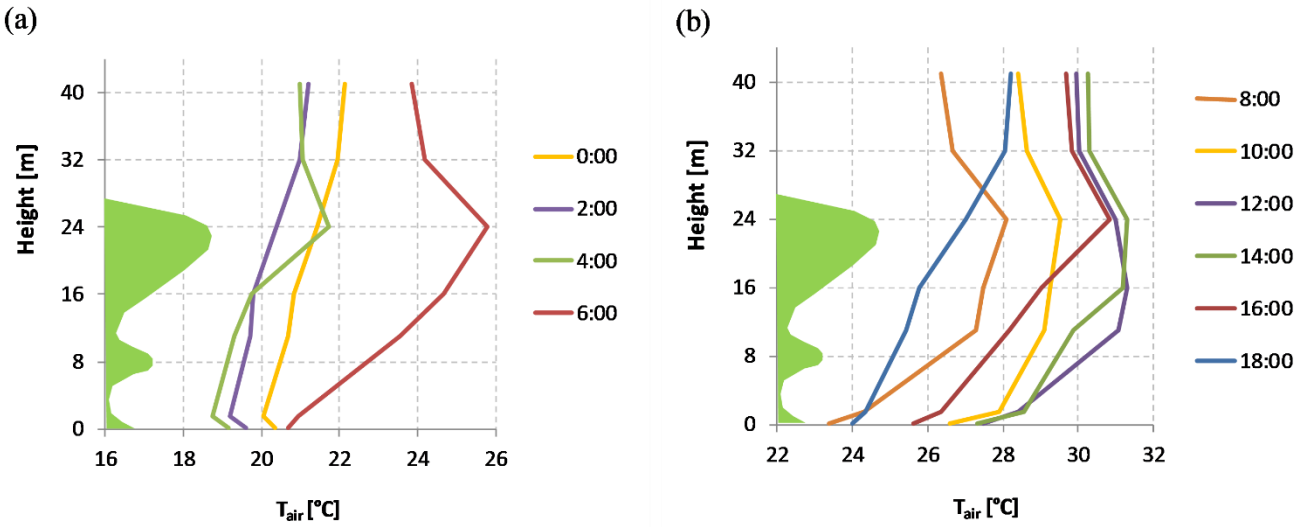

Figure 2 - Diurnal evolution of vertical profile of air temperature. (a) from 0:00 to 6:00; (b) from 8:00 to 18:00. The green shaded area represents the vertical distribution of the leaf area density expressed as m^2_{leaf} / m^3_{air} (= LAI / m_{height}).

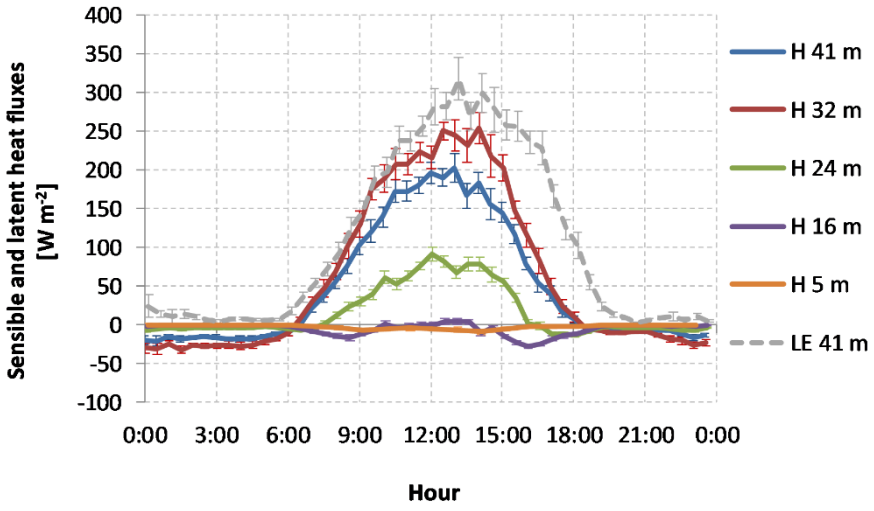

Figure 3 - Average diel course of sensible heat fluxes at the five levels (41 m, 32 m, 24 m, 16 m and 5 m, thick lines) and latent heat flux at 41 m (dashed line). Vertical bars represent the standard error of the mean.

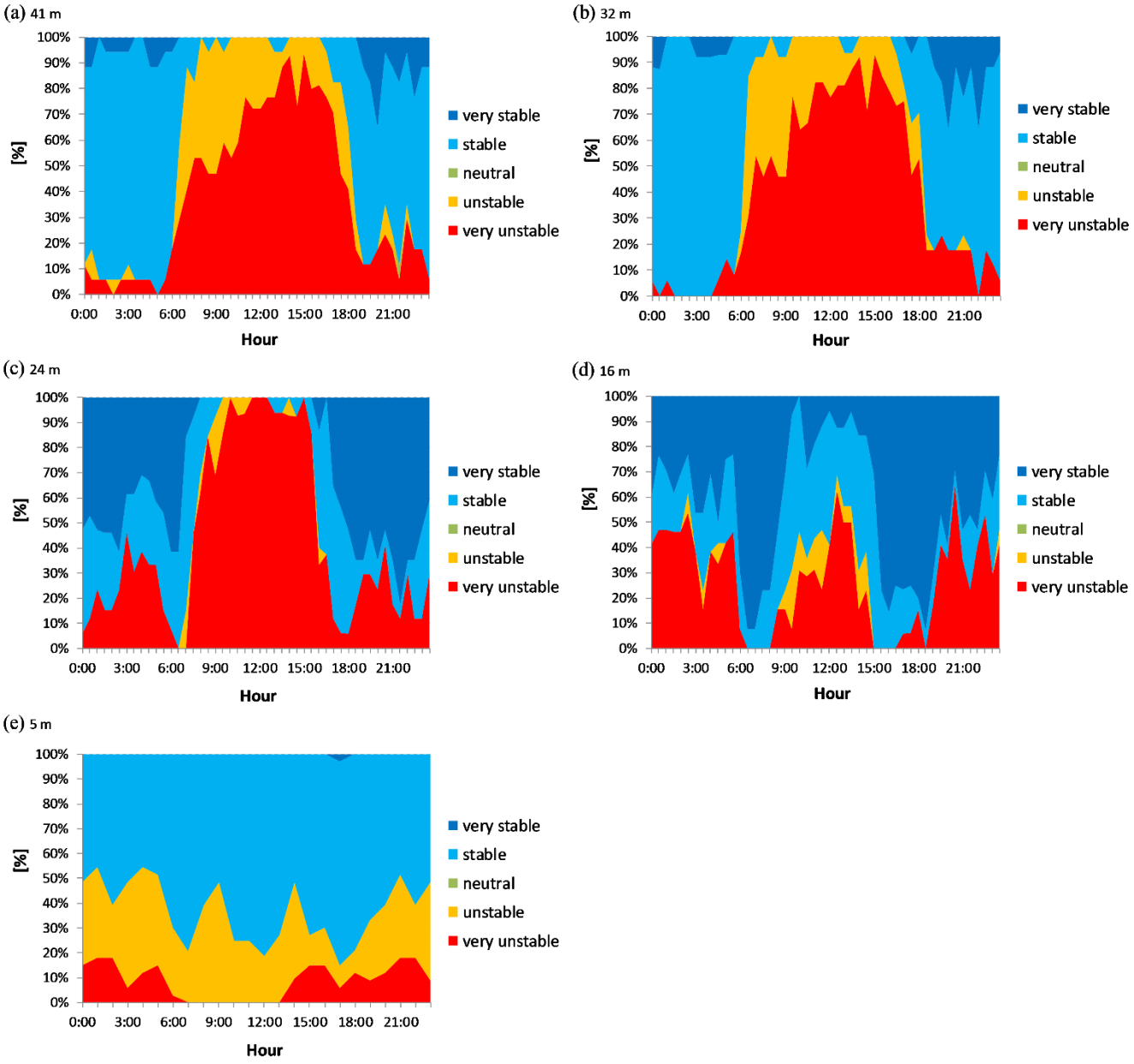

Figure 4 - Stability class distributions in the different hours of the day expressed as function of z/L for the different levels: (a) 41 m, (b) 32 m, (c) 24 m and (d) 16 m (e) 5 m. z is the measuring height while L is the Obukhov length. The stability classes were classified as follows according to Gerosa et al. (2017): very stable: $0<L\leq10$; stable: $10<L\leq100{,}000$; neutral: $|L|>100{,}000$; unstable: $-100{,}000\leq L<-100$; very unstable: $-100\leq L<0$.

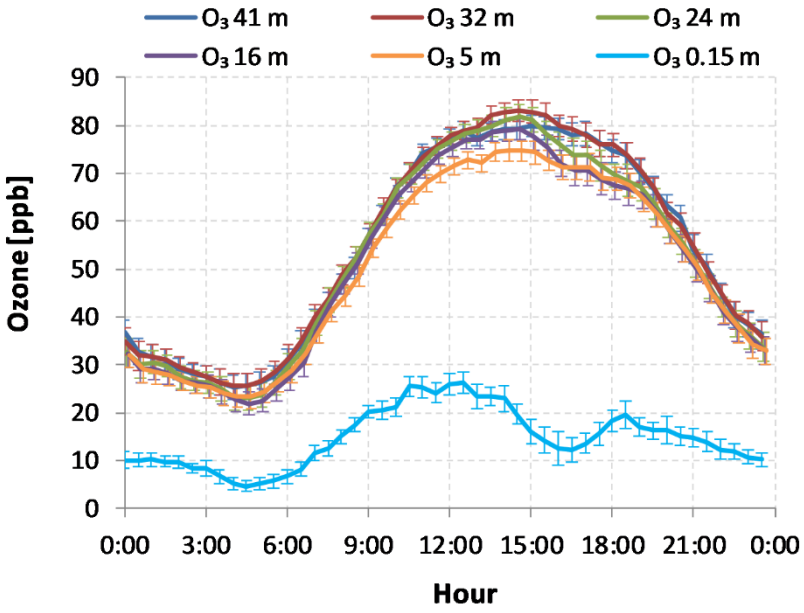

Figure 5 - Average diel courses of O_3 concentrations at six levels (41 m, 32 m, 24 m, 16 m, 5 m and 0.15 m). Vertical bars represent the standard error of the mean.

5

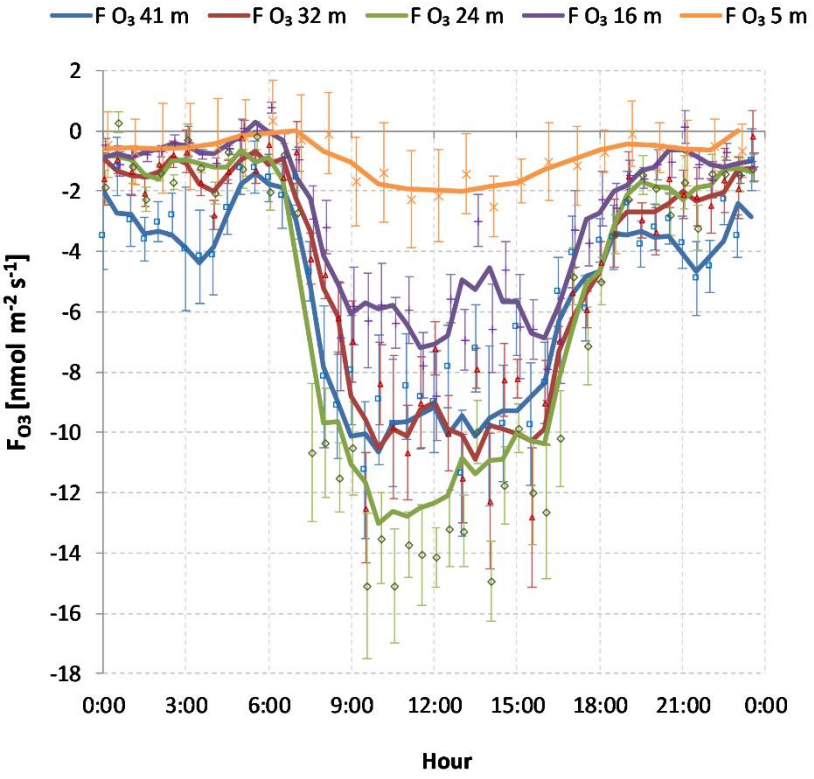

Figure 6 - Average diel courses of O_3 fluxes at five levels (41 m, 32 m, 24 m, 16 m and 5 m). Dots represent half-hourly averages while lines are one hour and half running means centered on each half hour. Vertical bars represent the standard error of the mean.

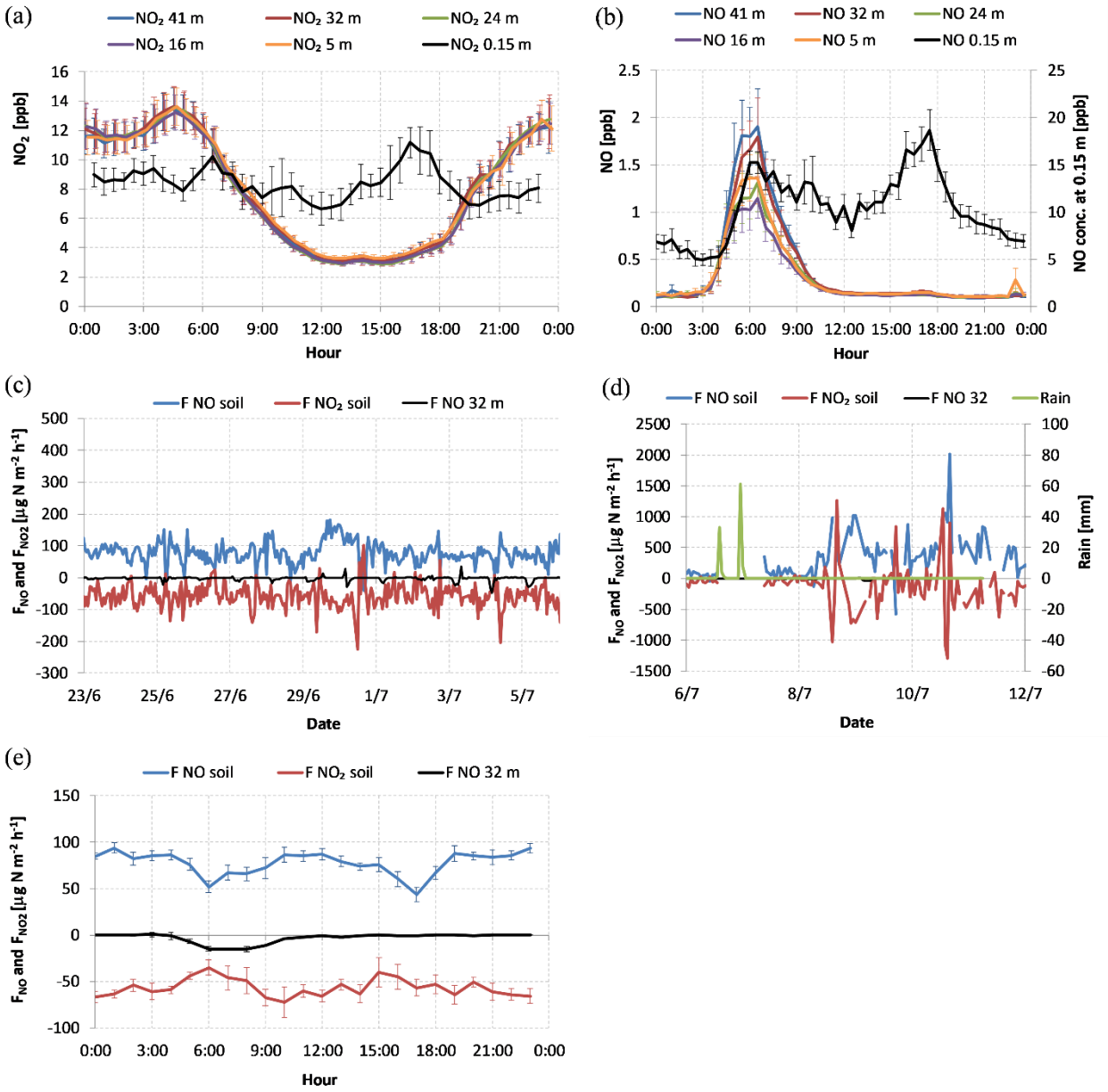

Figure 7 - Fluxes and concentrations of NO and NO_2. (a) Average diel course of NO_2 concentrations at the five levels (41 m, 32 m, 24 m, 16 m and 5 m); (b) Average diel course of NO concentrations; c) Soil NO and NO_2 fluxes and NO fluxes at 32 m before rainfalls events; (d) Soil NO and NO_2 fluxes and NO fluxes at 32 m after rainfall events (green line); (e) Average diel course of soil NO and NO_2 fluxes and of NO fluxes at 32 m. Please, note the different scale between (c) and (d). Vertical bars in (a), (b) and (e) represent the standard error of the mean.

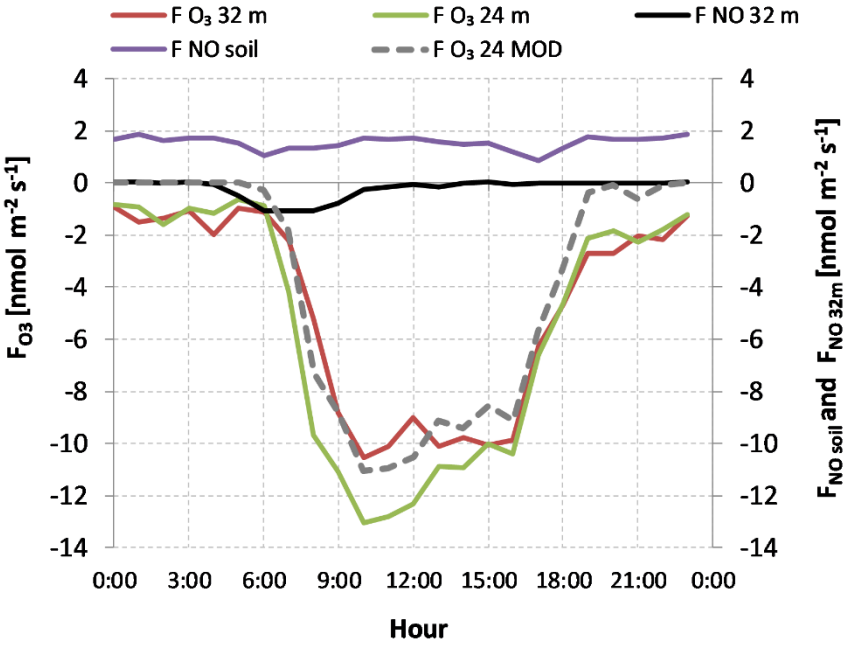

Figure 8 - Average diel course of O_3 fluxes at 32 m (red line), O_3 fluxes at 24 m (green line), NO fluxes at 32 m (black line), NO fluxes at soil level (purple line) and the modified (MOD) O_3 fluxes at 24 m (dashed grey line). This latter takes into account the role of the NO-related sink.

5

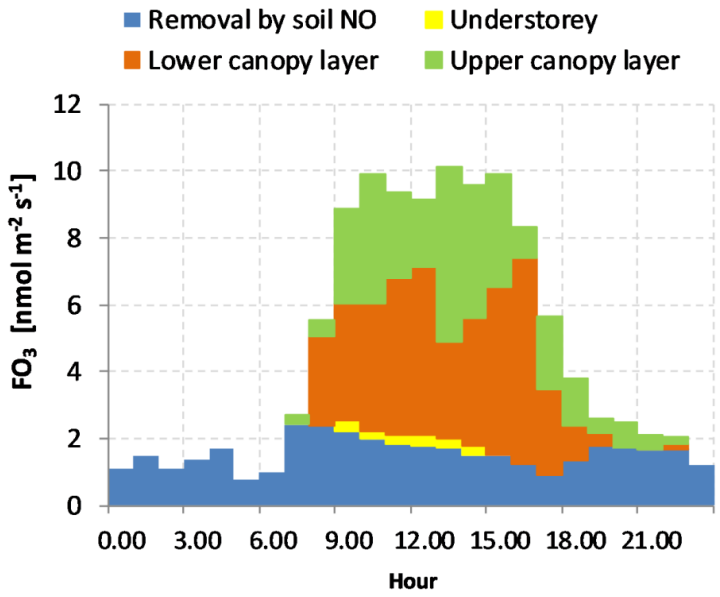

Figure 9 - Average diel course of the O_3 removal by the different forest layers and by the NO emitted from the forest floor.

5

Supplementary material

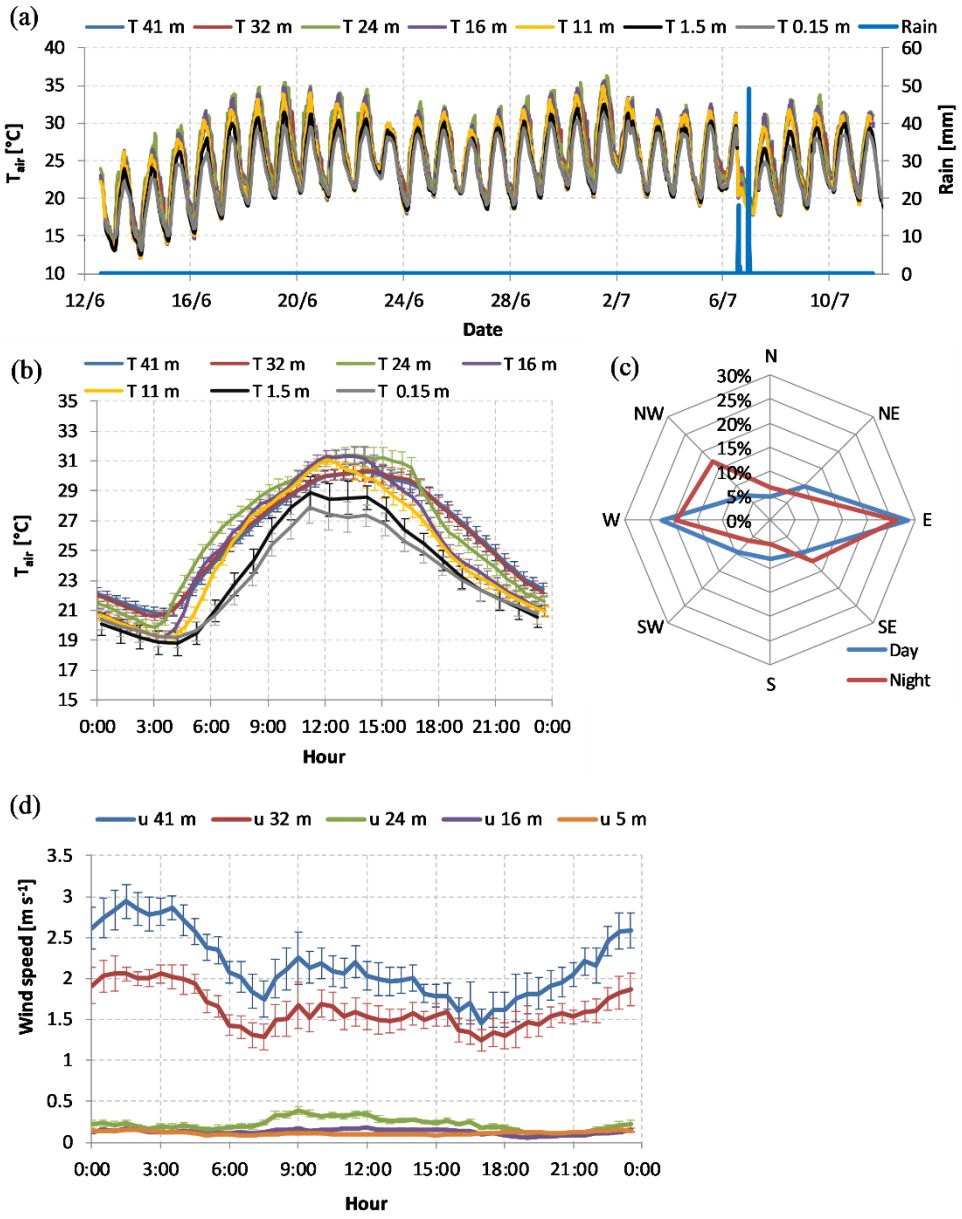

Figure S1 – (a) Rainfall amounts and temperature evolution at seven heights. Blue histograms are rainfalls. (b) Average diel course of air temperature at the seven heights. (c) Wind rose based on 41 m data, the radial axis unit indicates the percentage of the data in each direction, the blue line are diurnal data, the red line are nighttime data. (d) Average diel course of wind intensity at the five levels. Vertical bars in (b) and (d) represent the standard error of the mean.

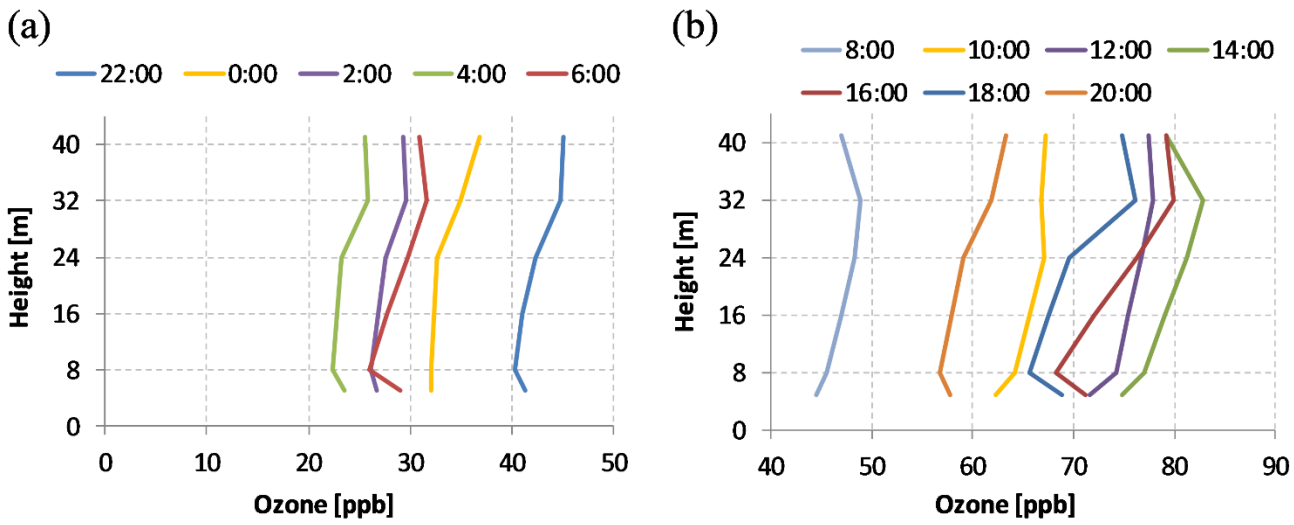

Figure S2 - Diurnal evolution of O_3 concentration profiles: (a) from 22:00 to 6:00; (b) from 8:00 to 20:00. The time of the day to which measurements are referred is indicated in each figure label. The 0.15 m level has not been included here for a better visualization (O_3 concentration at this level was around 10 ppb in (a) and below 25 ppb in (b)).

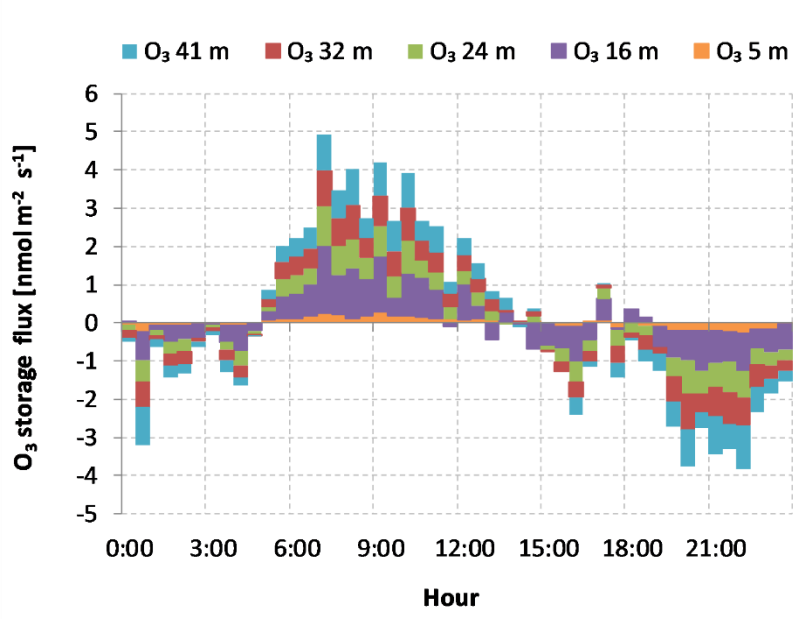

Figure S3 - Mean diel evolution of the O_3 storage flux (the storage term of the Eq. 3). The contribution of the air column between adjacent flux measurement levels is indicated with a different color.

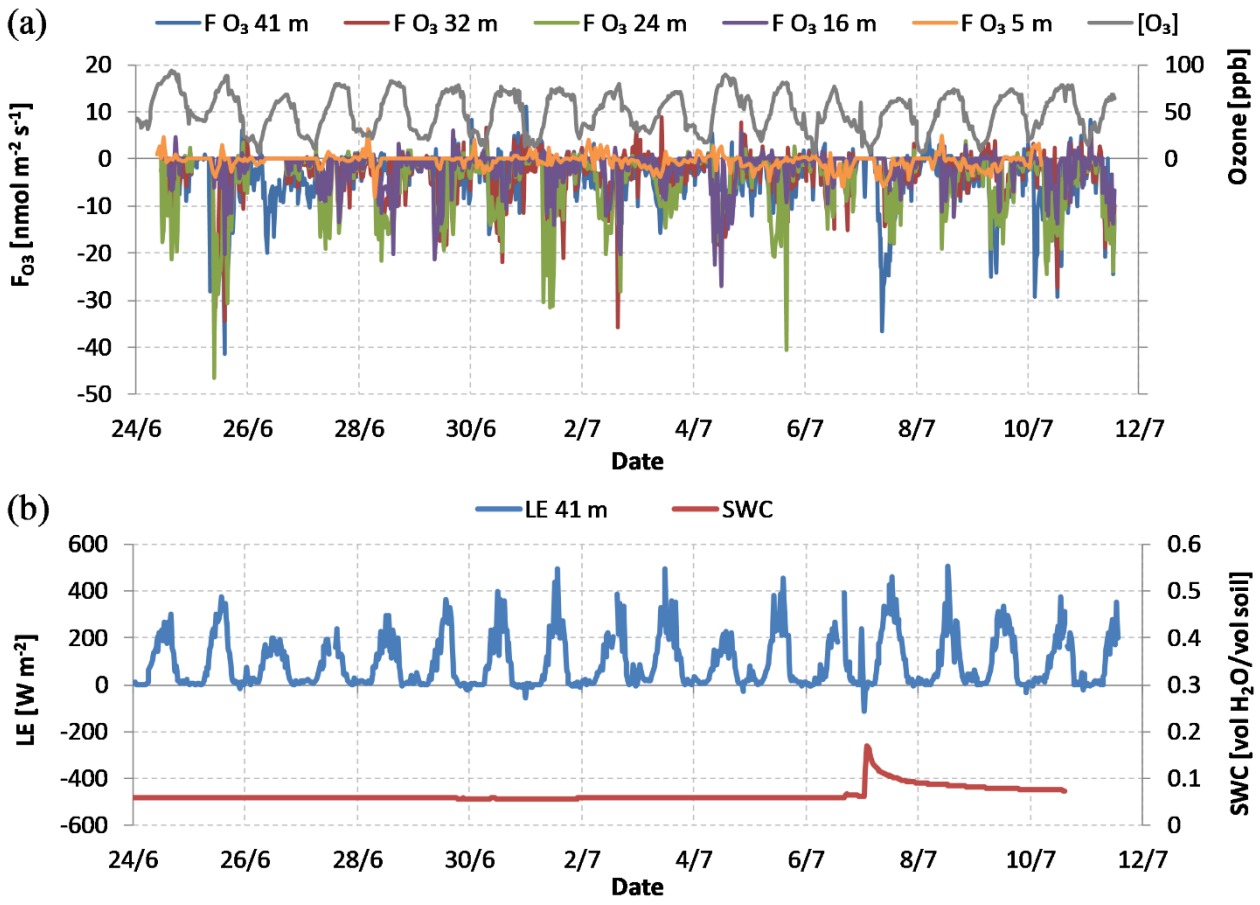

Figure S4 – (a) Ozone fluxes at the five levels (41 m, 32 m, 24 m, 16 m and 5 m) and ozone concentration at 41 m. (b) Latent heat fluxes measured at the top of the tower (LE 41) and soil water content (SWC) expressed as volumetric ratio between water and soil.

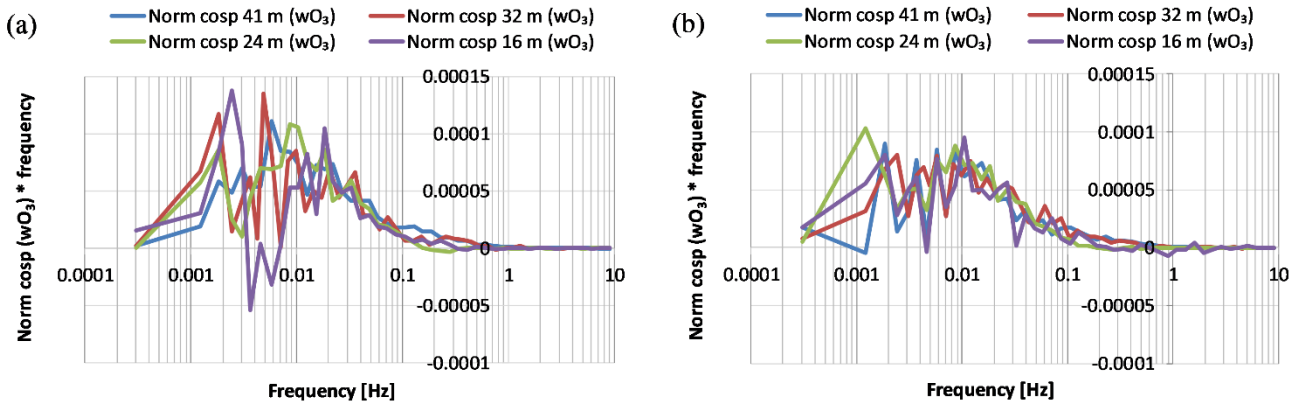

Figure S5 - Average normalized cospectra of the vertical component of the wind and O_3 at 11:00 (a) and at 15:00 (b).